Cell Reports

Article

Non-canonical Hedgehog signaling mediates profibrotic hematopoiesis-stroma crosstalk in myeloproliferative neoplasms

Graphical abstract

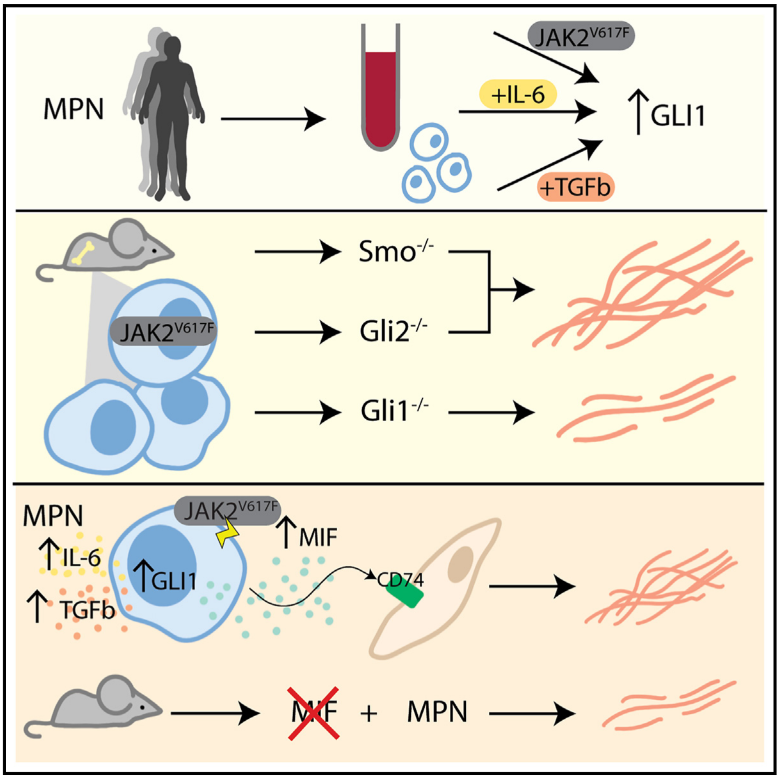

Highlights

- Gli1 protein levels in blood cells mark fibrotic progression in MPN patients
- Hematopoietic Gli1 is upregulated in a smoothened-independent manner in MPNs
- Gli1 mediates profibrotic crosstalk with stromal cells via MIF-CD74 axis
- Inhibiting Gli1 or MIF reduces MPN phenotype and fibrosis grade

Authors

Jessica E. Pritchard, Juliette E. Pearce, Inge A.M. Snoeren, ..., Hélène F.E. Gleitz, Rafael Kramann, Rebekka K. Schneider

Correspondence

reschneider@ukaachen.de

In brief

Pritchard et al. show that increased Gli1 protein levels in MPN patient blood cells mark fibrotic progression. By systematically interrogating the role of canonical vs. non-canonical Hedgehog signaling, they show that smoothened-independent hematopoietic Gli1 signaling is critical for profibrotic crosstalk with stromal cells via an MIF-CD74 axis.

Pritchard et al., 2024, Cell Reports *43*, 113608
January 23, 2024 © 2023 The Authors.
https://doi.org/10.1016/j.celrep.2023.113608

CellPress

Cell Reports

CellPress
OPEN ACCESS

Article

Non-canonical Hedgehog signaling mediates profibrotic hematopoiesis-stroma crosstalk in myeloproliferative neoplasms

Jessica E. Pritchard,[1,2,3] Juliette E. Pearce,[1] Inge A.M. Snoeren,[2,3] Stijn N.R. Fuchs,[2,3] Katrin Götz,[1] Fabian Peisker,[4] Silke Wagner,[1] Adam Benabid,[1] Niklas Lutterbach,[1] Vanessa Klöker,[5] James S. Nagai,[5] Monica T. Hannani,[4,6] Anna K. Galyga,[1] Ellen Sistemich,[1] Bella Banjanin,[2,3] Niclas Flosdorf,[1] Eric Bindels,[7] Kathrin Olschok,[8,9] Katharina Biaesch,[8,9] Nicolas Chatain,[8,9] Neha Bhagwat,[10] Andrew Dunbar,[11] Rita Sarkis,[12] Olaia Naveiras,[12] Marie-Luise Berres,[9,13] Steffen Koschmieder,[8,9] Ross L. Levine,[11] Ivan G. Costa,[5] Hélène F.E. Gleitz,[2,3] Rafael Kramann,[4,14,15] and Rebekka K. Schneider[1,2,3,16,*]

[1]Institute for Cell and Tumor Biology, RWTH Aachen University Hospital, Aachen, Germany
[2]Department of Developmental Biology, Erasmus University Medical Center, Rotterdam, the Netherlands
[3]Oncode Institute, Erasmus University Medical Center, Rotterdam, the Netherlands
[4]Institute of Experimental Medicine and Systems Biology, RWTH Aachen University Hospital, Aachen, Germany
[5]Institute for Computational Genomics, RWTH Aachen University Hospital, Aachen, Germany
[6]Institute for Computational Biomedicine, Heidelberg University Hospital, Heidelberg, Germany
[7]Department of Hematology, Erasmus Medical Center, Rotterdam, the Netherlands
[8]Department of Hematology, Oncology, Hemostaseology, and Stem Cell Transplantation, RWTH Aachen University Hospital, Aachen, Germany
[9]Center for Integrated Oncology Aachen Bonn Cologne Düsseldorf (CIO ABCD), Aachen, Germany
[10]Prelude Therapeutics, Wilmington, DE, USA
[11]Human Oncology and Pathogenesis Program, Leukemia Service, Department of Medicine, Memorial Sloan Kettering Cancer Center, New York, NY, USA
[12]Laboratory of Regenerative Hematopoiesis, Department of Biomedical Sciences (DSB), Université de Lausanne (UNIL), Lausanne, Switzerland
[13]Medical Department III, RWTH University Hospital Aachen, Aachen, Germany
[14]Department of Internal Medicine, Nephrology and Transplantation, Erasmus University Medical Center, Rotterdam, the Netherlands
[15]Department of Nephrology and Clinical Immunology, RWTH Aachen University Hospital, Aachen, Germany
[16]Lead contact
*Correspondence: reschneider@ukaachen.de
https://doi.org/10.1016/j.celrep.2023.113608

SUMMARY

The role of hematopoietic Hedgehog signaling in myeloproliferative neoplasms (MPNs) remains incompletely understood despite data suggesting that Hedgehog (Hh) pathway inhibitors have therapeutic activity in patients. We aim to systematically interrogate the role of canonical vs. non-canonical Hh signaling in MPNs. We show that Gli1 protein levels in patient peripheral blood mononuclear cells (PBMCs) mark fibrotic progression and that, in murine MPN models, absence of hematopoietic *Gli1*, but not *Gli2* or *Smo*, significantly reduces MPN phenotype and fibrosis, indicating that GLI1 in the MPN clone can be activated in a non-canonical fashion. Additionally, we establish that hematopoietic *Gli1* has a significant effect on stromal cells, mediated through a druggable MIF-CD74 axis. These data highlight the complex interplay between alterations in the MPN clone and activation of stromal cells and indicate that *Gli1* represents a promising therapeutic target in MPNs, particularly that Hh signaling is dispensable for normal hematopoiesis.

INTRODUCTION

Primary myelofibrosis (PMF) is a myeloproliferative neoplasm (MPN) characterized by the replacement of hematopoietic tissue in the bone marrow (BM) with fibrotic scar tissue. Despite extensive research into genetic alterations in hematopoietic stem cells (HSCs) that lead to MPNs and PMF,[1–4] the mechanisms by which the fibrosis-driving niche cells are transformed and activated are not yet fully understood.

Recent work has demonstrated that *Gli1*, a downstream effector transcription factor (TF) of the Hedgehog (Hh) signaling pathway marks a population of non-hematopoietic stromal cells as a critical population of fibrosis-driving cells, not only in PMF[5] but also in solid organs.[6,7] The Hh signaling pathway is highly conserved, with a critical role in development,[8] and includes three ligands (Indian, sonic, and desert Hh), the receptor PTCH1, the transmembrane protein smoothened (SMO), and the downstream TF family of Gli proteins. Dysregulation of this tightly controlled pathway has been implicated in the development of a number of cancer types,[9] including MPNs.[10]

While data show that targeting the Hh pathway at the level of SMO has clinical benefits in some cancer treatments,[11] and SMO inhibition is US Food and Drug Administration (FDA) approved for basal cell carcinoma (BCC), effectiveness in patients with MPN is varied.[12–15] Importantly, these studies showed that *GLI1* expression is still upregulated after treatment with SMO inhibitors,[12] indicating that *GLI1* can be upregulated in an SMO-independent fashion. Pre-clinical data indicate that direct GLI1/2 targeting is effective in murine models of PMF,[5] suggesting that non-canonical Hh signaling in MPN may be more prevalent. We define non-canonical signaling here as activation of Gli proteins independent of upstream SMO. The role of canonical vs. non-canonical Hh signaling has never been systematically analyzed in PMF.

We here hypothesized that inhibition of Hh/Gli signaling in hematopoietic cells may ameliorate BM fibrosis (BMF) and potentially interrupt crosstalk with fibrosis-driving stromal cells. Our data reveals that GLI1 in the MPN clone can be activated in a non-canonical fashion and may represent a therapeutic target, in particular because we confirm that Hh signaling is dispensable for normal HSC function and hematopoiesis.[16,17]We demonstrate that hematopoietic *Gli1* has a significant effect on stromal cells in fibrosis, mediated through a patient-relevant MIF-CD74 axis.

RESULTS

GLI1, but not SHH, is deregulated on a protein level in peripheral blood from patients with MPNs

First, we examined the activity of Hh signaling in the peripheral blood (PB) of patients with MPNs, given that increased *GLI1* mRNA levels have been found in MPN stromal cells and granulocytes.[5,18] We performed an ELISA for sonic Hh protein (SHH), a canonical ligand of the Hh pathway, on plasma samples from healthy donors (HDs) and patients with MPN (Table S1). We found no correlation between SHH concentration and disease status (Figure 1A).

We next asked whether there is a link between the JAK2^{V617F} mutation and increased *GLI1* mRNA. The JAK2^{V617F} mutant SET-2 cell line had significantly increased *GLI1* transcripts compared with the JAK2^{WT} MEG-01 cell line (Figure 1B). This link between the mutation and increased transcript levels was confirmed in induced pluripotent stem cell (iPSC) lines derived from patients with MPNs when comparing JAK2^{WT} and JAK2^{V617F} clones (Figure 1C).

To investigate whether transcriptional changes seen in granulocytes from JAK2^{V617F} patients with MPNs[18] are reflected in altered protein levels, we performed intracellular fluorescence-activated cell sorting (FACS) on PB mononuclear cells (PBMCs) to determine GLI1 protein levels (Figure S1A). The CD66b^{HI} population had a significantly increased mean fluorescence intensity (MFI) for GLI1 in patients with fibrosis (grade 1) and marked the onset of fibrosis compared with both HDs and patients without fibrosis (grade 0) (Figure 1D). Importantly, the increased GLI1 protein expression did not solely correlate with the increased numbers of CD66b^{Hi} cells (Figure S1B).

In CD88$^+$/89$^+$ monocytes, which are decreased in number in patients with MPNs (Figure S1C), a similar pattern of GLI1 increase occurs at onset of fibrosis (Figure 1E). There was a trend for GLI1 protein to be expressed at lower levels in MF0 than in HDs and significantly lower than in MF1.

Altered lymphocyte levels in patients with MPNs have been reported previously[19,20] and were confirmed in our cohort (Figures S1D and S1E). In our cohort, GLI1 levels in T cells were significantly correlated with onset of fibrosis, and the same trend was seen in the B cell population (Figure 1F).

To link the increased GLI1 protein levels seen in PBMCs from patients with MPNs to non-canonical stimulation of the Hh pathway, we isolated PBMCs from HDs and stimulated them with MPN-relevant cytokines: TGFb1[21,22] or interleukin-6 (IL-6).[22–24] After 72 h of stimulation, TGFb1 and IL-6 resulted in increased GLI1 levels in CD66b$^+$ granulocytes (Figure 1G), and TGFb1 increased GLI1 levels in CD19$^+$ B cells (Figure S1F).

Our data indicate that GLI1 expression is cell type specific, is differentially regulated throughout the course of MPNs, and increases with the onset of BMF. The increase in GLI1 protein levels between MF0 and MF1 in multiple hematopoietic lineages independent of cell number changes suggests that Hh signaling via GLI1 within hematopoietic cells plays a role in the progression of non-fibrotic MPNs to overt fibrotic disease. These data, when taken together with previous data showing an increase in *GLI1* expression in fibrosis-driving stromal cells,[5] suggest a role of GLI1 in both the hematopoietic and stromal niches in MPNs.

Knockout of Gli1 in hematopoietic cells reduces BMF

To investigate the role of hematopoietic GLI1 in MPNs, we utilized two methods of BMF induction: overexpression of thrombopoietin (ThPO) and *Jak2^{V617F}*. After lethal irradiation, mice received a transplantation (Tx) of either wild-type [WT] or *Gli1$^{-/-}$* germline knockout cKit$^+$ hematopoietic stem and progenitor cells (HSPCs) transduced with either the overexpression/mutation vector or its corresponding control (Figures 2A and S2A).

Jak2^{V617F} overexpression first recapitulates the myeloproliferative phase of MPNs mainly characterized by polycythemia.[25,26] When the disease progresses to fibrosis, blood counts and hemoglobin (Hgb) levels drop reflecting the inability of fibrotic BM to produce mature blood cells. Although *Gli1* knockout in *Jak2^{V617F}*-overexpressing HSPCs did not ameliorate increased Hgb levels, it prevented the progressive anemia typically seen in this model with advanced fibrosis (Figure 2B). In line, *Gli1* knockout in HSPCs in the *Jak2^{V617F}* setting also prevented a decrease in platelet (PLT) levels over time. Although GLI1 levels are increased in granulocytes in patients with MPN with progressive disease grades, *Gli1* knockout in HSPCs did not affect white blood cell (WBC) counts.

Our analysis of the PB indicated that absence of *Gli1* is not sufficient to fully ameliorate the *Jak2^{V617F}*-induced MPN phenotype but that mice do retain more normal hematopoietic function than those with *Gli1*. *Jak2^{V617F}* overexpression in HSPCs lead to changes in the HSC compartment, specifically an increase in long-term (LT) HSCs (Lin$^-$Sca1$^+$cKit$^+$ [LSK], CD48$^-$ CD150$^+$) (Figure 2C). Inhibition of *Gli1* reduced this expansion to normal levels. Using GFP as a marker, we quantified the number of *Jak2^{V617F}* mutant LT HSCs in the BM (Figure 2D). These are

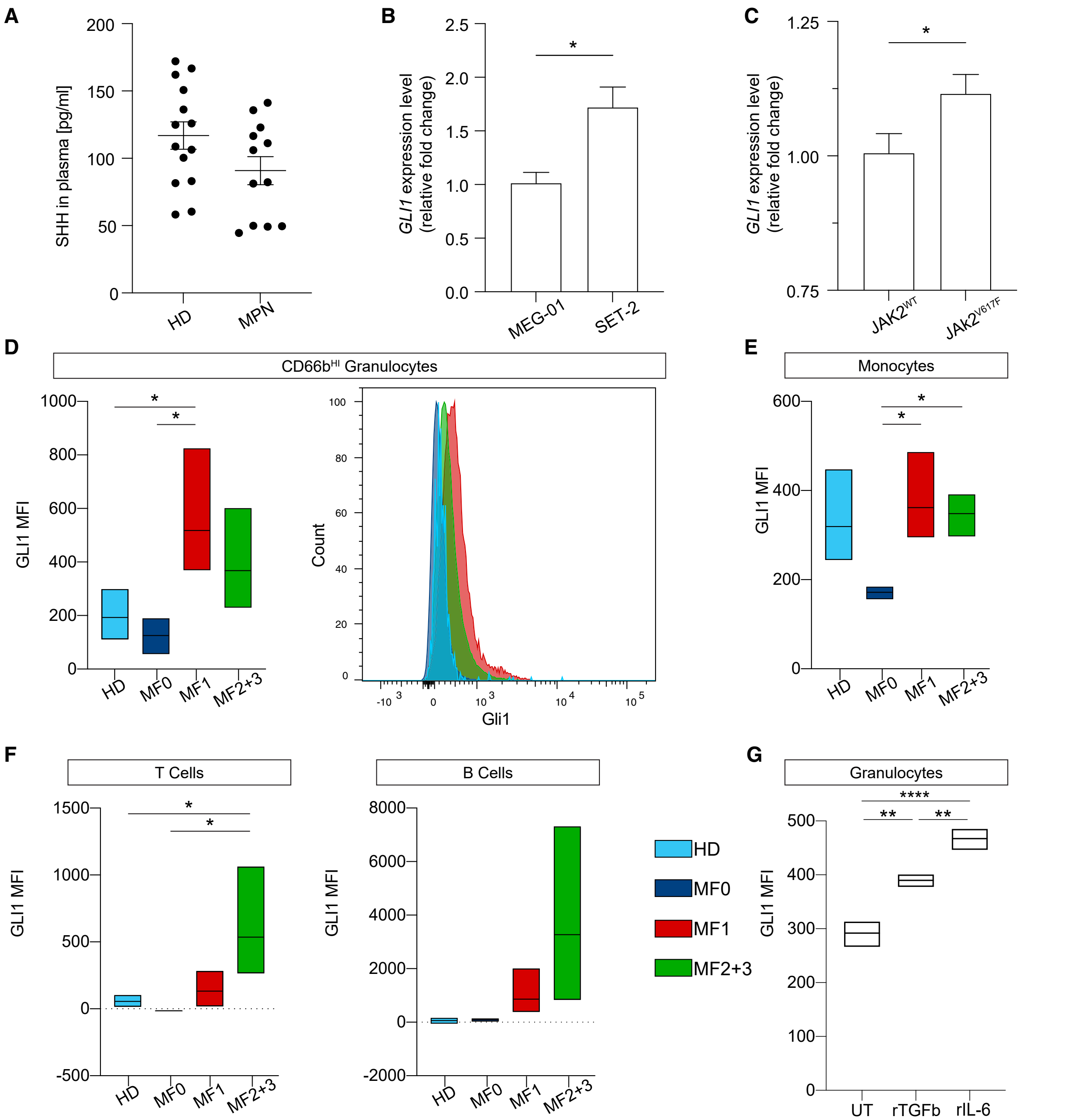

Figure 1. SHH levels remain normal in patients with MPNs, while *GLI1* RNA and protein level increases are linked to the *JAK2^{V617F}* mutation

(A) Plasma from patients with MPNs (n = 12, IDs MPN1–MPN12) and healthy donors (HDs) was isolated, and SHH protein levels were determined by ELISA.

(B) *GLI1* expression in megakaryocytic cell lines was quantified with qPCR relative to *GAPDH*, and the *JAK2^{V617F}*-containing SET2 cell line was normalized to the *JAK2^{WT}* MEG-01 cell line (n = 3).

(C) *GLI1* expression in undifferentiated patient-derived iPSC lines was quantified with qPCR relative to *GAPDH*, normalized to respective *JAK2^{WT}* clones (n = 3).

(D) PBMCs isolated from patients with MPNs compared with HD samples (HDs, n = 4, n = 5; MF0, n = 3; MF1, n = 4; MF2 and MF3, n = 3, IDs MPN13–MPN22). Shown are MFI quantification of GLI1 levels in CD66b^{HI} granulocytes per group normalized to fluorescence minus one (FMO) controls and a representative GLI1 histogram, with count normalized to mode.

(E and F) MFI quantification of GLI1 levels per group normalized to FMO controls in CD88^{+}CD89^{+}HLADR^{+} monocytes (E), CD3^{+} T cells, and CD19^{+} B cells (F).

(G) MFI quantification of GLI1 levels in CD66b^{+} granulocytes after PBMCs from HDs (n = 3) were stimulated with 10 ng/mL rTGFb or 50 ng/mL rIL-6 for 72 h, normalized to FMO controls.

Bar chart data are shown as mean ± SEM with unpaired Student's t test. Boxplot data are shown as minimum (min) to maximum (max) with line at mean, one-way ANOVA followed by Tukey's post hoc test. *p < 0.05, ** = p < 0.01, **** = p < 0.0001. See also Figure S1 and Table S1.

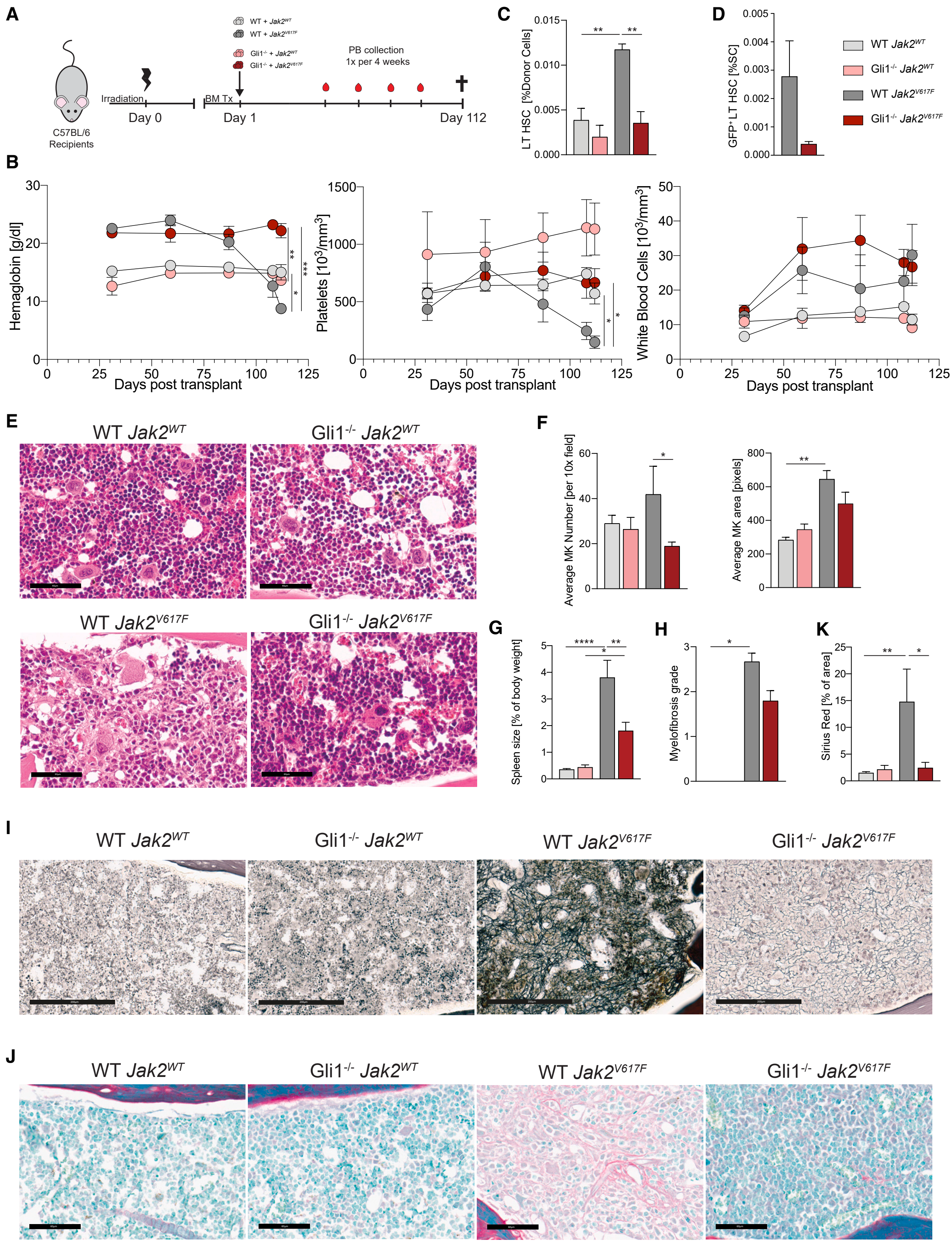

(legend on next page)

reduced in the absence of *Gli1*, suggesting that *Gli1* plays a role in the clonal expansion of a *Jak2*^{V617F} HSCs BM. The absence of *Gli1* in normal HSPCs only leads to a minor, nonsignificant reduction of the LT HSC fraction, indicating that it may be an attractive therapeutic target for the specific reduction of the disease-causing clone.

Another typical feature of *Jak2*^{V617F}-induced MPNs is increased megakaryocyte number and size. H&E staining showed this pathognomonic megakaryocyte morphology with clustering of hyperlobulated megakaryocytes in atypical locations (Figure 2E). In striking contrast, in the absence of *Gli1*, the BM showed erythroid hyperplasia, in line with increased Hgb levels, but megakaryocytes that were more comparable in morphology and frequency with healthy BM (Figures 2E and 2F). The absence of *Gli1* in the non-diseased background affected neither morphology nor cellularity (Figure 2E). Consistent with the progressed MPN phenotype, in WT *Jak2*^{V617F} mice, the spleen-to-body weight ratio was significantly increased, indicating increased levels of extramedullary hematopoiesis (Figure 2G), and hematopoietic knockout of *Gli1* in *Jak2*^{V617F}-mediated MPNs reduced this.

As expected from the advanced splenomegaly in the presence of *Gli1* in *Jak2*^{V617F}-induced disease, the BM showed progressed fibrosis (Figure 2H). In contrast, *Gli1*$^{-/-}$*Jak2*^{V617F} BM had low-grade fibrosis (Figure 2I). This was also phenocopied in the ThPO model, where the absence of *Gli1* resulted in fibrosis no greater than grade 1 compared with grade 2–3 with *Gli1* (Figure S2E), although there was no accompanying effect on other measures of disease severity in the PB or BM (Figures S2B–S2D). Hematopoietic *Gli1* knockout also preserved the cellularity of the BM in *Jak2*^{V617F}-induced disease (Figure S2F). Importantly, there was no significant difference in the overall GFP^{+} percentage observed in the BM at sacrifice between the WT JAK2^{V617F} and *Gli1*$^{-/-}$JAK2^{V617F} conditions, indicating that the observed phenotype reduction was not due to a reduced number of transduced cells in the BM (Figure S2H).

To definitively demonstrate that *Gli1*$^{-/-}$ results in less advanced fibrosis, we performed Sirius red/fast green staining, which stains collagen I and, thus, highlights more advanced fibrosis. Strikingly, only sections of femora from WT *Jak2*^{V617F} mice stained positive, while in the *Gli1*$^{-/-}$ setting, red-stained collagen fibers were only observed around the central arteries itself (Figure 2J). This difference was significant (Figure 2K), and the absence of hematopoietic *Gli1* in *Jak2*^{V617F}-induced fibrosis normalized the amount to baseline levels. This is further evidence that, in the absence of *Gli1*, fibrosis is reduced in both *Jak2*^{V617F} and ThPO overexpression models of BMF.

Important for future therapeutic prospects, we observed no negative hematopoietic phenotype in mice transplanted with *Gli1*$^{-/-}$ HSPCs compared with WT HSPCs. While changes were observed in the stem cell compartment of the BM (Figure S2G), engraftment was unaffected (Figure S2H). To further confirm that targeting GLI1 would not result in reduced stem cell fitness, we performed a competitive transplantation using a 50:50 mix of *Gli1*$^{-/-}$ and WT BM (Figure S2K). After 152 days, we observed no significant difference in engraftment or stem cell compartments between the two BM genotypes (Figures S2L and S2M), confirming that loss of *Gli1* does not have a detrimental effect on HSC function.

Neither knockout of Gli2 nor SMO in hematopoietic cells is sufficient to ameliorate the PMF phenotype

We asked whether the reduction in *Jak2*^{V617F}-mediated fibrosis seen in the absence of *Gli1* also occurred in the absence of *Gli2*, another effector TF in the Hh signaling pathway shown to play a critical role in kidney fibrosis.[27] We investigated whether the reduction of fibrosis seen in the absence of *Gli1* could be recapitulated by knocking out the upstream canonical regulator of *Gli1* and *Gli2*, *Smo*, which would strongly argue for a role of canonical Hh signaling via the three Hh ligands and *Ptch1*. WT mice were transplanted with either WT, *Gli2*, or *Smo* knockout HSPCs that had been transduced with the Jak2^{V617F} patient-relevant mutation plasmid or the WT control (Figure S3A).

Gli2$^{-/-}$ mice still developed an MPN phenotype comparable with the WT *Jak2*^{V617F} condition. Hgb, WBC, and PLT levels remained increased compared with controls and, in the case of WBCs, even trended higher throughout the experiment (Figure 3A), suggesting that hematopoietic *Gli2* is not a key player in myelofibrosis. Smo knockout in the *Jak2*^{V617F} setting did not significantly ameliorate the MPN phenotype, and the onset of anemia and reduction in PLTs indicated worsening BM function (Figure 3A). Neither knockout affected engraftment of the BM (Figure S3B).

Figure 2. Loss of *Gli1* in HSPCs reduces BMF

(A) C57BL/6 mice received lethal irradiation followed by WT or *Gli1*$^{-/-}$ cKit^{+} HSPCs transduced with *Jak2*^{V617F} or WT control retroviral vectors (n = 5/group). Mice were sacrificed at 112 days after transplantation.

(B) Hgb, PLT, and WBC counts from PB over the course of the experiment. Mean ± SEM, two-way ANOVA with Geisser-Greenhouse correction followed by Tukey's post hoc test; significance for values at sacrifice is indicated.

(C) FACS quantification of the long-term hematopoietic stem cell (LT HSC; Lin^{-}Sca1^{+}cKit^{+} CD48^{-}CD150^{+}) population as a percentage of the Lin^{-}Sca1^{+}cKit^{+} (LSK) fraction in BM.

(D) FACS quantification of GFP^{+} LT HSC population as a percentage of all single cells (SCs) in the BM.

(E) Representative images of H&E staining. Scale bar, 60 μm.

(F) Quantification of megakaryocyte number and area in BM from H&E staining of the femur.

(G) Weight of the spleen at sacrifice as a percentage of total body weight.

(H) Quantification of myelofibrosis grade based on reticulin staining of the femur.

(I) Representative images of reticulin staining. Scale bar, 200 μm.

(J) Representative images of Sirius red/fast green staining of the femur. Scale bar, 60 μm.

(K) Quantification of Sirius red staining as a percentage of total area from Sirius red/fast green staining of the femur.

Bar chart data are shown as mean ± SEM, one-way ANOVA followed by Tukey's post hoc test. *$p < 0.05$, **$p < 0.01$,*** = $p < 0.001$,****$p < 0.0001$. See also Figure S2.

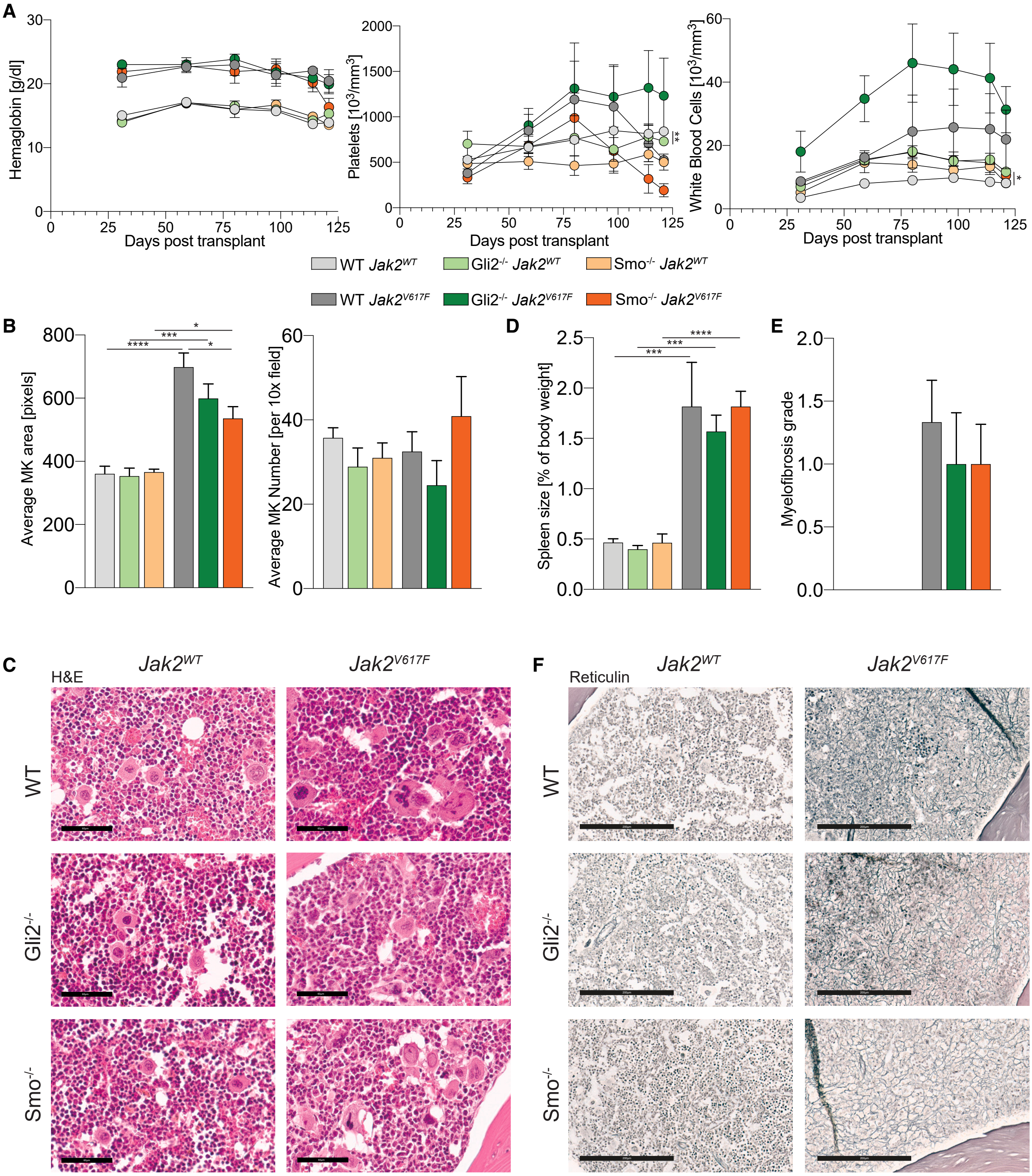

Figure 3. Loss of *Gli2* or *Smo* in HSPCs does not reduce MPN or fibrotic phenotype

C57BL/6 recipient mice received lethal irradiation followed by WT, *Gli2*$^{-/-}$, or *Smo*$^{-/-}$ cKit^{+} HSPCs, isolated 4 weeks after final poly(I:C) injection, transduced with *Jak2*^{V617F} or WT control retroviral vectors (n = 5/group). Mice were sacrificed 112 days after transplantation.

(A) Hgb, PLT, and WBC counts from PB over the course of the experiment. Mean ± SEM, two-way ANOVA with Geisser-Greenhouse correction followed by Tukey's post hoc test; significance for values at sacrifice is indicated.

(B) Quantification of megakaryocyte number and area in BM from H&E staining of the femur.

(C) Representative images of H&E staining of the femur. Scale bar, 60 μm.

(legend continued on next page)

Significantly altered BM architecture was observed in *Jak2*^{V617F}-induced MPNs in all genotypes. Megakaryocyte size was reduced in the absence of *Smo* and *Gli2*, but typical features of dysplasia remained (Figures 3B and 3C). In healthy BM, the knockout of *Gli2* and *Smo* did not significantly influence the BM architecture compared with the control condition (Figure 3C).

Neither knockout of *Gli2* nor *Smo* was sufficient to reduce *Jak2*^{V617F}-induced extramedullary hematopoiesis, as measured by spleen-to-body weight ratio. (Figure 3D). In line with this, neither *Gli2* nor *Smo* knockout ameliorated reticulin fibrosis in the BM, and all mice with *Jak2*^{V617F}-induced fibrosis, regardless of genotype, presented with grade 1–2 fibrosis (Figures 3E and 3F). Quantification of collagen I in these mice also did not indicate any reduction in fibrosis level in the absence of *Gli2* or *Smo*. The finding of no fibrosis or MPN phenotype improvement was recapitulated in the ThPO model (Figures S3D–S3F).

While the lack of fibrosis reduction without *Gli2* or *Smo* eliminates them as potential therapeutic targets, the absence of an effect on normal hematopoiesis is additional evidence that targeting the pathway, via modulating GLI1 activity in patients, is a viable option. These findings further indicate that *Gli1* can be activated independent of canonical Hh signaling via *Smo* because only knockout of *Gli1* but not *Smo* ameliorates the MPN phenotype and fibrosis. Therefore, our data strongly indicated that non-canonical activation of *Gli1* is an important mechanism driving myelofibrosis.

Gli1 mediates transcription of MPN-associated genes in HSPCs

Because *Gli1* seems to play a role in the regulation of MPNs independent of canonical *Smo* activation, we next dissected the role of *Gli1* in hematopoiesis by performing single-cell RNA sequencing (scRNA-seq) on BM cells in *Jak2*^{V617F}-induced fibrosis and control, both in the presence and absence of *Gli1*. To understand the transcriptional changes occurring in the HSPC populations, we analyzed lineage-depleted, whole BM obtained at the end of a transplantation experiment in MPNs (Figure 2A). At time of sacrifice, all *Jak2*^{V617F} mice in the presence of *Gli1* in HSPCs showed progressed MPNs and high-grade BMF, while mice in the absence of *Gli1* had only low-grade BMF (Figure 2I).

Unsupervised clustering revealed 13 hematopoietic cell types and one non-hematopoietic stromal cluster (Figure 4A; Tables S2 and S3).[28–30] The top five differentially expressed genes (DEGs) per cluster demonstrate the commonalities between related clusters (Figure S4A; Table S4), and each condition (*Gli1* WT vs. *Gli1*$^{-/-}$) was represented in each cluster (Figure S4B). Investigation of the stromal compartment revealed two subpopulations: a mesenchymal stromal cell (MSC)-like and a fibroblast-like population (Figure S4C). This observation is consistent with heterogeneity seen in previously published stromal scRNA-seq datasets.[29,31]

We first explored the role of Gli1 in normal hematopoiesis by examining the DEGs in HSPCs. Our previous work demonstrated that S100A8 is elevated in MPNs and that targeting of S100A8/S100A9 signaling ameliorates BMF.[26] Strikingly, *S100a8* was among the top differentially downregulated genes with significantly reduced expression in the HSC and common myeloid progenitor (CMP) 3 cluster in the absence of *Gli1* (Figure 4B); additionally, this is also seen across myeloid-lineage clusters (Figure S4D). We did not observe an impairment of myeloid differentiation in the absence of *Gli1* in our mouse models (Figures S2I and S2J). Furthermore, in the CMP3 cluster, *S100a11* was significantly downregulated in the absence of *Gli1* (Figure 4B). S100A11 is linked to activation of the WNT/β-catenin pathway[32] and the release of IL-6 from neutrophils,[33] factors that have been linked to MPNs.[34,35] Among the differentially upregulated genes in some of the most stem-cell-like populations were many ribosome-associated genes (Figure 4B), suggesting increased protein translation in the absence of *Gli1*.

Next, we investigated changes associated with *Gli1* in the *Jak2*^{V617F}-induced MPN setting, focusing on the primitive HSPC clusters. Notably, Hgb subunits (*Hbb-bs* and *Hbb-bt*) were downregulated in the absence of *Gli1* in the HSC, CMP1, and CMP3 clusters (Figure 4C). Increased expression of *Hbb* has been linked to increased survival of metastasis-competent circulating tumor cells in solid organs,[36] perhaps indicating a link between *Gli1* and the increased proliferation and survival of the malignant clone in MPN. This also correlates with compensatory erythropoiesis seen in advanced fibrosis in MPNs. Another striking alteration is the downregulation of *Lgals1* (Galectin-1) in *Jak2*^{V617F}-induced MPNs in without *Gli1*. Galectin-1 has been linked to inflammation and extracellular matrix production, both signatures key to solid organ fibrosis and MPNs.[37–39] Similar patterns of expression of ribosome-associated genes were associated with the absence of *Gli1* (Figure 4C).

These data so far suggest that *Gli1*$^{-/-}$, in addition to mediating transcription of MPN-associated genes, does not lead to detrimental expression changes in the most primitive HSPC compartments under normal conditions, providing further evidence that modulating GLI1 in patients with MPNs would specifically target the malignant clone.

TF analysis reveals cell-type-specific Gli family member expression patterns

Functional redundancy exists within the Gli TF family,[40] and a systematic examination of the role of the members (GLI1, GLI2, and GLI3) in MPNs has not been done previously. Therefore, we performed network analysis using the Discriminant Regulon Enrichment Analysis (DoRothEA) tool[41] to analyze TF activity in the HSC and CMP3 clusters (Figure 4D). There was little differential activity in the HSC cluster between the control and

(D) Weight of the spleen at sacrifice as percentage of total body weight.
(E) Quantification of myelofibrosis grade based on reticulin staining of the femur.
(F) Representative images of reticulin staining. Scale bar, 200 μm.
Bar chart data are shown as mean ± SEM, one-way ANOVA followed by Tukey's post hoc test. *p < 0.05, **p < 0.01, ***p < 0.001, ****p < 0.0001. See also Figure S3.

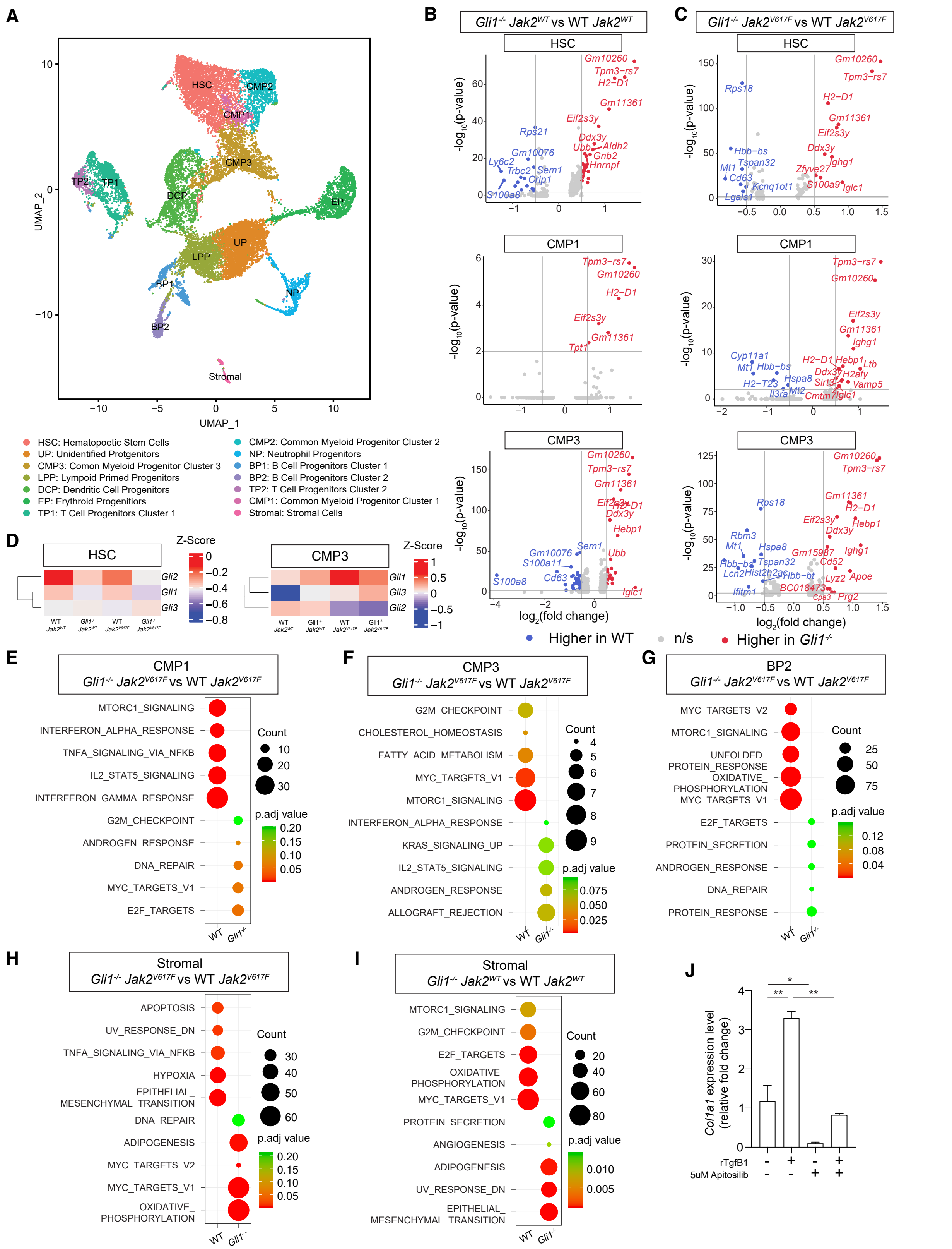

(legend on next page)

$Jak2^{V617F}$-induced MPN settings, indicative of the tight regulation of the Hh pathway in HSPCs. As confirmation of our knockout, the activity of GLI1 was down under both *Gli1*$^{-/-}$ conditions. Unexpectedly, *Gli1*$^{-/-}$ led to increased activity of GLI3 in $Jak2^{V617F}$-mediated fibrosis. Given the opposite function of these two family members (activating and repressive, respectively), this is unlikely to be due to functional redundancy between the two. In the more differentiated progenitor cluster, CMP3, there is a significant increase in GLI1 activity (Figure 4D) in control $Jak2^{V617F}$-induced disease conditions, in line with myeloid cells from patients with MPNs exhibiting higher GLI1 RNA and protein levels (Figures 1D–1F).

Gli1 differentially regulates pathways known to be perturbed in MPNs in HSPCs

To identify signaling pathways that are differentially regulated by *Gli1* in $Jak2^{V617F}$-mediated fibrosis, we performed gene set enrichment analysis (GSEA) using Hallmark gene sets.[42] Pathways known to be important in $Jak2^{V617F}$-induced MPNs are in the top 5 gene sets significantly associated with fibrosis in the presence of *Gli1*, including the tumor necrosis factor alpha (TNF-α)[26] and WNT[34] signaling pathways (Figure 4E; Table S5). Pathways involving interferon response and JAK-STAT signaling are central pathways in the pathogenesis of MPNs[3] and are significantly upregulated in $Jak2^{V617F}$-induced fibrosis in the presence of *Gli1* (Figure 4E), indicating that targeting GLI1 in patients with MPNs would potentially reduce the activation of these pathways and thus reduce disease burden. The absence of *Gli1* in HSPCs generally led to induction of pathways such as DNA repair but also pathways indicative of increased proliferation of HSCs, such as E2F (Figure 4E).

Because $JAK2^{V617F}$ mutations arise in the primitive HSPC compartment and result in myeloid biased differentiation, the mutation is typically found in myeloid cells.[43] However, in patients, they are also known to be present in lymphoid cells.[43,44] In our data, key MPN pathways, such as TNF-α and WNT, were found similarly altered in both lymphoid clusters and myeloid clusters (Figure 4G; Table S5).

One of the most striking repeated signatures was the upregulation of gene sets linked to the phosphatidylinositol 3-kinase (PI3K) pathway, such as mTORC1 signaling, which is significantly associated with the presence of *Gli1* in $Jak2^{V617F}$-mediated fibrosis (Figures 4E–4G). The PI3K/AKT/mTOR pathway has been shown previously to be activated by *Gli1* in poor-prognosis acute myeloid leukemia patients,[45] and, conversely, PI3K has been shown to activate *Gli1* in a noncanonical fashion,[46] providing evidence that targeting PI3K rather than SMO might also be an attractive strategy to inhibit *Gli1* activation and the Hh signaling cascade in MPNs.

Each of these patterns is indicative of the milder phenotype seen in $Jak2^{V617F}$-induced fibrosis in the absence of *Gli1* and provides insight into possible benefits of targeting GLI1 independent of canonical Hh signaling in MPNs.

Pathway changes occur in stromal cells in response to the presence of hematopoietic Gli1

Importantly, due to the transplant model and techniques used, the stromal compartment in this dataset is both unmutated and WT for *Gli1* expression. Therefore, any transcriptional changes identified must occur due to alterations in *Gli1*-dependent communication from the transplanted donor HSPCs. To investigate the downstream effects of hematopoietic *Gli1* on $Jak2^{V617F}$-induced fibrosis, we also performed GSEA on this stromal cluster (Figures 4H and 4I; Table S5) using Hallmark gene sets.[42]

Of note, stromal cells exposed to $Jak2^{V617F}$ BM cells had significantly upregulated hypoxia-associated genes. This is a known signature of fibrosis[47] and was reduced in the absence of hematopoietic *Gli1* (Figure 4H). Stromal cells also showed upregulation of Hallmark gene sets associated with epithelial-to-mesenchymal transition, TNF-α, and apoptosis (Figure 4H). This supports a more fibrotic, dysregulated stromal niche in the presence of hematopoietic $Jak2^{V617F}$ and *Gli1* and suggests that, in the absence of hematopoietic *Gli1*, stromal cells are less primed for fibrotic transformation.

Under both the disease and healthy conditions, the Adipogenesis Hallmark gene set in the stromal cluster was more associated with the absence of hematopoietic Gli1. We thus used MarrowQuant[48] to quantify adipose tissue in the marrow from these mice and did not find any significant differences in adipose tissue area (Figure S4E). However, we found a significant reduction in adipocyte density in the non-disease marrow in the absence of hematopoietic Gli1 compared with the WT condition (Figure S4F), an interesting topic for future studies.

Based on data from the hematopoietic clusters (Figures 4E–4G), we hypothesized that the mechanism of action behind PI3K inhibitor success in patients with MPN[49,50] is not solely due to the effect on the disease-causing malignant clone because PI3K is upstream of mTORC1/2 signaling.[51] To validate the role of the PI3K/mTORC1 signaling axis in fibrosis driving stromal cells, we used the robust *in vitro* model of stimulating

Figure 4. scRNA-seq analysis reveals the role of Gli1 in pro-fibrotic gene expression and pathway activation

(A) Unsupervised clustering of scRNA-seq of whole BM collected at sacrifice (112 days post Tx) from mice transplanted with either WT or *Gli1*$^{-/-}$ cKit$^+$ HSPCs transduced with either $Jak2^{V617F}$ or WT control retroviral vectors (n = 3/group, n = 19,897 cells) and identification of 13 hematopoietic clusters and 1 non-hematopoietic cluster.

(B) Volcano plots of DEGs, *Gli1*$^{-/-}$ versus WT in control, HSC, CMP1, and CMP3 clusters. Wilcoxon rank-sum test, two tailed; calculated individually per cluster.

(C) Volcano plot of *Gli1*$^{-/-}$ versus WT in $Jak2^{V617F}$ fibrosis in HSC, CMP1, and CMP3 clusters.

(D) Heatmap representation of Discriminant Regulon Enrichment Analysis (DoRothEA) of Gli-family TFs in HSC and CMP1 clusters.

(E–H) Top 5 (p.adj) Hallmark terms identified by GSEA comparing *Gli1*$^{-/-}$$Jak2^{V617F}$ and WT$Jak2^{V617F}$ conditions for the (E) CMP1, (F) CMP3, (H) BP2, and (I) stromal clusters.

(I) Top 5 (p.adj) Hallmark terms identified by GSEA for the stromal cluster, comparing *Gli1*$^{-/-}$$Jak2^{WT}$ and WT$Jak2^{WT}$ conditions.

(J) hBM-MSC cell line pre-treated with 5 μM apitosilib or DMSO control and then treated and co-stimulated with 10 ng/mL rTGFB1 for 48 h. *COL1a1* expression was quantified with qPCR relative to *HPRT1*, normalized to the unstimulated, untreated condition (n = 3).

Mean ± SEM, one-way ANOVA followed by Tukey's post hoc test. *p < 0.05, **p < 0.01. See also Figure S4 and Tables S2–S5.

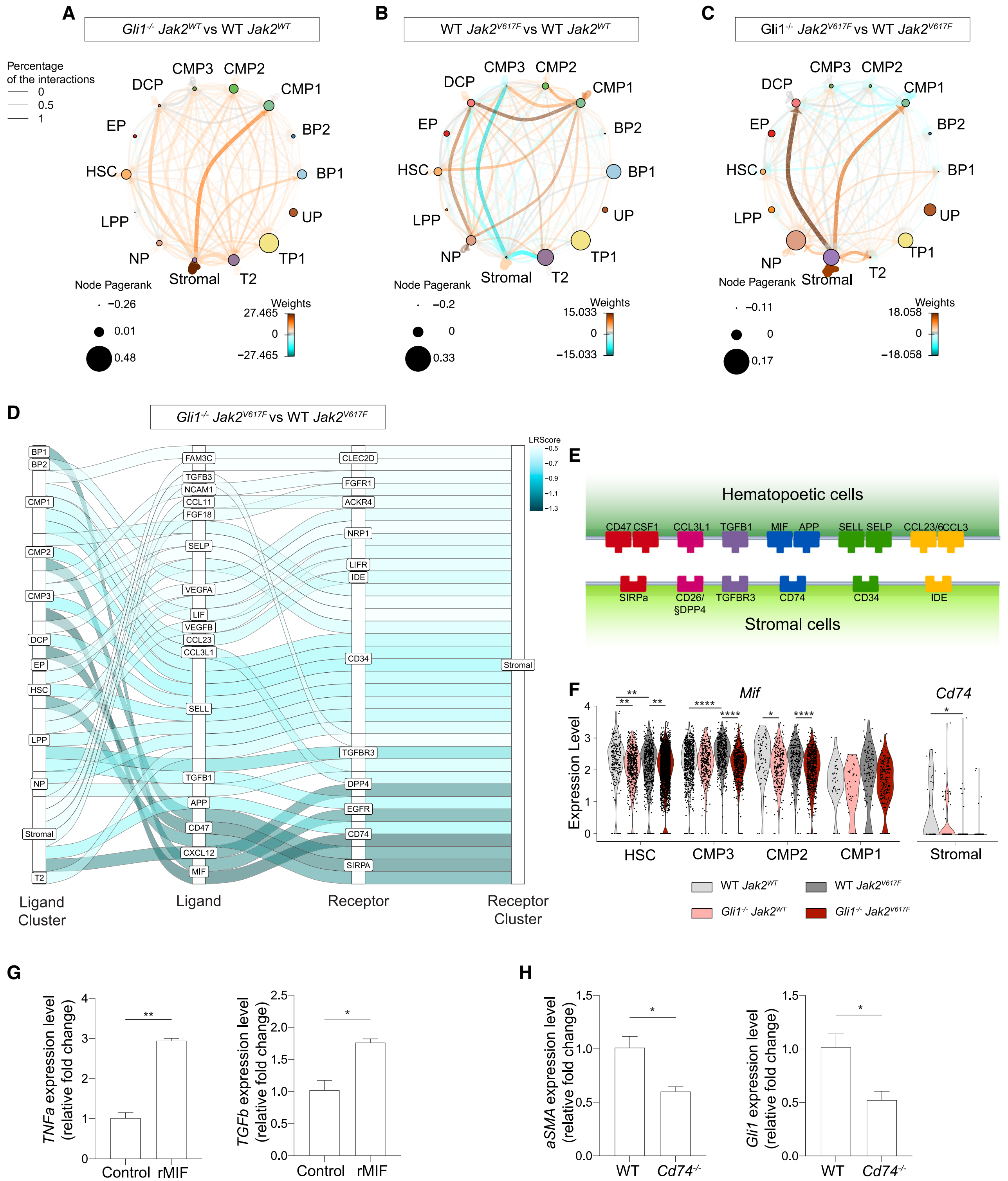

Figure 5. Ligand-receptor analysis shows change in interactions via the disease-relevant MIF-CD74 axis

(A–C) Network plots of ligand-receptor (LR) activity comparing (A) the *GLI1*$^{-/-}$ condition and WT in the non-disease setting, (B) the *Jak2*^{V617F} and WT conditions, and (C) the *GLI1*$^{-/-}$*Jak2*^{V617F} and *WTJak2*^{V617F} conditions.

(D) Top 35 downregulated interactions based on stromal cluster receptors in *GLI1*$^{-/-}$ *Jak2*^{V617F} compared with WT *Jak2*^{V617F}; interactions are ordered based on LRScore.

(legend continued on next page)

BM-derived MSCs (BM-MSCs) with recombinant transforming growth factor β 1 (rTGFB1). Stimulation of BM-MSC with rTGFB1 for 48 h led to a significant 3-fold increase in expression of *Col1a1* (collagen 1), which is a well-known readout of fibrosis in BM-MSCs (Figure 4J), relative to unstimulated controls. When the cells were treated with 5 μM of the pan-PI3K and mTORC1/2 inhibitor apitosilib, *Col1a1* was significantly downregulated even after stimulation with rTGFB1 compared with stimulated, untreated BM-MSCs.

Ligand-receptor analysis shows rewired hematopoietic-stromal cell communication in the absence of hematopoietic Gli1

Previous research has indicated an important role for the hematopoietic-stromal cell crosstalk in MPN and fibrosis initiation and progression.[25,26,52] Thus, we wanted to investigate what these interactions are and how they change with hematopoietic *Gli1* expression.

Using CrossTalkeR,[53] we compared cell-cell interactions under non-disease conditions to examine the role of *Gli1* in homeostasis (Figure 5A; Table S6). In general, there were more significant interactions between almost all cell clusters in the absence of *Gli1*, and of particular interest was the highly increased level of self-interaction within the stromal cell cluster. This finding could indicate that hematopoietic *Gli1* regulates a wide range of cellular crosstalk even in homeostasis.

We next evaluated cell-cell interaction changes in $Jak2^{V617F}$-induced disease progression in the presence of *Gli1* (Figure 5B). The general pattern was a loss of many interactions, particularly between hematopoietic cell clusters and the stromal cluster, indicative of the complete dysregulation of normal BM function and loss of stroma-derived hematopoietic support that occurs in $Jak2^{V617F}$-induced fibrosis. Interestingly, the clusters with more increased interactions were the neutrophil progenitors (NPs) and CMP1 and CMP2, indicative of a myeloid-derived immune cell involvement in fibrosis. This is in contrast with the CMP3 cluster, which appears to have significantly fewer interactions with many cell types. Given previous evidence of this cluster having reduced *S100a8* expression in the absence of *Gli1* (Figure 4B) and also the significant differences in Gli-family TF activity (Figure 4D), these data highlight the importance of this CMP3 population in the progression of BMF in MPNs.

To evaluate the contribution of hematopoietic *Gli1* to these $Jak2^{V617F}$-mediated changes in cell-cell interaction, we compared the *Gli1* knockout $Jak2^{V617F}$ and WT $Jak2^{V617F}$ conditions (Figure 5C). Decreased intercellular interactions seem to be associated with worse fibrosis grade, and increased interactions are associated with the milder phenotype seen in the absence of hematopoietic *Gli1*. These data show that the absence of *Gli1* results in increased interactions between the stromal cluster and various hematopoietic cell types, suggesting a less deregulated marrow. It also shows the same pattern of increased self-interaction in the stromal cluster. Of particular note are the increased interactions between the stromal cell cluster and the previously noted CMP3 cluster.

The disease-relevant hematopoietic MIF-to-stromal CD74 axis is modulated by Gli1

To further interrogate the mechanisms behind the role of *Gli1* in $Jak2^{V617F}$-mediated fibrosis, we focused on comparing the two disease states, where downregulated interactions are associated with worse fibrosis grade. Interrogating a ranking of the top downregulated ligand-stromal receptor pairs (Figure 5D, Table S6), we identified 6 receptors and 10 ligands shortlisted for further investigation (Figure 5E). The strongest downregulated interaction was the CMP3-MIF-CD74-stromal axis. The CMP3 cluster has highly altered interactions with stromal cells in normal disease development (Figure 5B). *Mif* expression was increased in $Jak2^{V617F}$-mediated fibrosis in the HSC, CMP3, and CMP2 clusters, and this was significantly reduced in the absence of *Gli1*. Additionally, in the $Jak2^{WT}$ settings, absence of *Gli1* reduced *Mif* expression in the HSC and CMP2 clusters. *Cd74* expression was reduced in stromal cells in fibrosis in the presence of hematopoietic *Gli1* (Figure 5F).

To confirm the disease relevance of the MIF-CD74 axis, we stimulated human MSCs with recombinant MIF and observed a significant increase in expression of the fibrosis-associated genes *TNFa* and *TGFb1* compared with unstimulated controls (Figure 5G). At the other side of the axis, when $Cd74^{-/-}$ murine MSCs were cultured with ThPO conditioned medium, they expressed significantly reduced levels of *aSMA* and *Gli1*, both known key markers of fibrotic stromal cells (Figure 5H).

MIF protein levels are relevant in patients with MPNs, and expression is linked to JAK2 and PI3K

We next validated that the *Gli1*-mediated MIF-CD74 axis is relevant to patients with fibrosis and may represent an attractive therapeutic target by collecting serum from patients with MPNs (Table S1) and performing a MIF ELISA (Figure 6A). MIF protein levels were indeed significantly increased in patients with MPNs compared with HDs, trending up in patients diagnosed with polycythemia vera and specifically significantly increased in patients with essential thrombocytopenia and PMF. Serum MIF levels were significantly correlated with PLT levels (Figure 6A), although no link to allele burden or fibrosis grade was observed (Figure S5A). Interestingly this is not

(E) Representation of LR interactions shortlisted for further interrogation.

(F) Violin plot of *MIF* expression across HSPC and myeloid primed clusters and of *Cd74* in the stromal cluster across all conditions. One-way ANOVA followed by Tukey's post hoc test.

(G) A human MSC cell line, MSOD, was stimulated with 100 ng/mL recombinant MIF for 24 h. *TNFa* and *TGFb* expression relative to HPRT1 expression was quantified by qPCR and normalized to the unstimulated condition. Unpaired Student's t test with Welch's correction (n = 3).

(H) BM-MSCs isolated from WT or $CD74^{-/-}$ mice were treated with conditioned medium collected from an immortalized BM progenitor cell line overexpressing ThPO to induce a fibrotic phenotype. *aSMA* and *GLI1* expression levels were quantified by qPCR and normalized to the WT stromal cells (n = 3). Unpaired Student's t-test with Welch's correction.

*p < 0.05, **p < 0.01, ****p < 0.0001. See also Table S6.

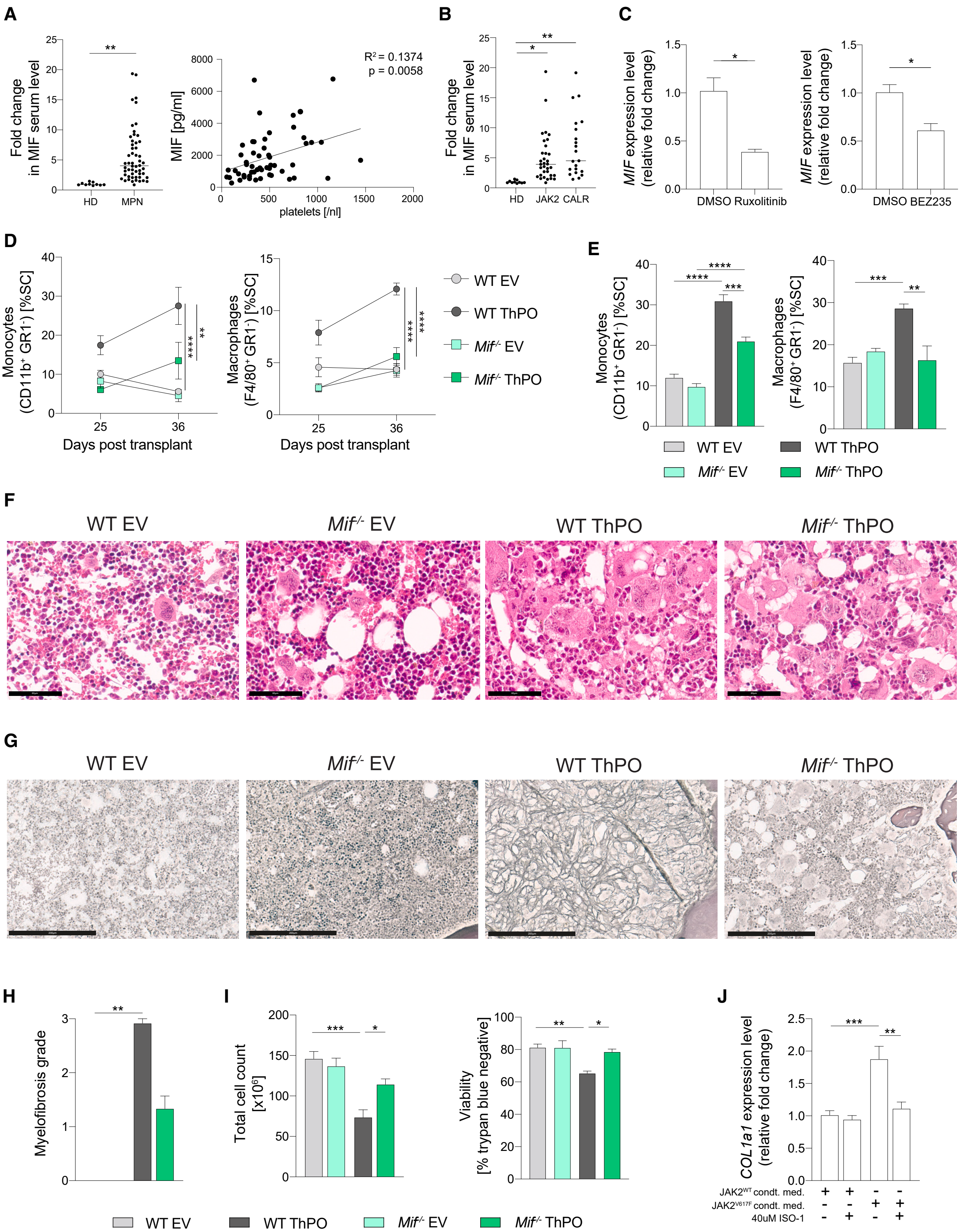

(legend on next page)

exclusive to patients harboring a JAK2^{V617F} mutation, and MIF protein levels are also significantly increased in patients with a calreticulin (CALR) mutation (Figure 6B), raising the possibility that therapeutic intervention targeting MIF would benefit a wide range of patients with MPNs.

To better understand the mechanism behind MIF expression in patients with MPNs, we utilized JAK2^{V617F} mutant HEL cells and treated them with either the JAK2 inhibitor ruxolitinib or the dual PI3K/mTOR inhibitor BEZ235.[54] In both cases, *Mif* mRNA expression was significantly reduced compared with untreated controls (Figure 6C).

Genetic or pharmacological perturbation of the MIF-CD74 axis reduces disease phenotype

Having shown the relevance of MIF in patients with MPNs and illustrated a potential mechanism of regulation, we next wanted to validate its potential as a therapeutic target. Utilizing the previously described ThPO overexpression MPN model, WT mice were transplanted with either WT of *Mif* knockout HSPCs that had been transduced with the ThPO overexpression vector or empty vector control (Figure S5B).

In the absence of MIF, mice transplanted with THPO overexpression BM exhibited many typical aspects of the MPN phenotype (Figures S5C–S5G). However, there were significant reductions in both monocytes and macrophages in the PB over time (Figure 6D) and in the BM at sacrifice (Figure 6E). The monocyte expansion typically seen in this model was ameliorated.

Whilst the absence of MIF in the ThPO overexpression mouse model did not completely normalize the MPN phenotype (Figures S5C–S5G and 6F), reticulin staining demonstrated a quantifiable reduction in reticulin fibrosis (Figures 6G and 6H), and this was coupled with normalization of BM cellularity and BM viability in the absence of MIF (Figure 6I). Importantly, there was no difference in engraftment of GFP expression in the marrow collected at sacrifice, confirming that the reduction of fibrosis is an MIF-dependent effect and not due to reduced gene marking (Figure S5D). Thus, we demonstrated that *Mif* knockout has a specific effect on the fibrosis-driving stroma and on reducing the pathognomonic monocytosis.

To confirm that pharmacologically targeting MIF can reduce the fibrotic transformation, we cultured a human MSC cell line with conditioned medium collected from iPSCs during myeloid differentiation of JAK2^{WT} or JAK2^{V617F} patient-derived iPSCs. When cultured with the JAK2^{V617F}-conditioned medium, key markers such as collagen 1 were significantly upregulated in the stromal cells compared with the control. With the addition of the MIF antagonist, ISO-1, this was normalized, indicating that MIF released from hematopoietic cells upregulates fibrosis genes in stromal cells and, importantly, that the upregulated MIF in patients is an attractive therapeutic target, either alone or in combination with JAK inhibition (ruxolitinib), to increase the inhibitory effect on MIF itself but also fibrosis (Figure 6J).

DISCUSSION

Our studies reveal a key role of non-canonical Hh signaling in the development and progression of PMF. We provide evidence that GLI1 can be a biomarker for disease progression and also a therapeutic target. While SHH protein levels in MPN patient serum are no different from that from HDs, *GLI1* expression levels are specifically increased in a JAK2^{V617F}-mutant megakaryocytic cell line and patient-derived IPSCs compared with the JAK2^{WT} equivalents. In addition, GLI1 protein levels are increased in both myeloid and lymphoid subsets of JAK2^{V617F} PBMCs isolated from patients with MPNs. Importantly, this change marks the transition from non-fibrotic MPNs to overtly fibrotic disease. While this finding requires validation in larger cohorts, intracellular GLI1 flow cytometry could be implemented in follow-up appointments of patients to assess progression.

Previous data indicate that Hh signaling is dispensable for normal hematopoiesis.[16,17,55] However, these studies either made use of *Smo* knockout mice[16,17] or analyzed hematopoietic cells in steady-state Gli1-null mice.[55] Because it is now widely accepted that the Gli family of TFs can be activated independent of Hh ligands, the use of upstream Hh pathway knockouts does

Figure 6. MIF protein levels are relevant in patients with MPNs, and genetic or pharmacological perturbation of the MIF-CD74 axis reduces disease phenotype

(A) MIF protein level assessed by ELISA in patients with MPNs (n = 54) was normalized to HD (n = 10) samples (IDs MPN23–MPN76). Unpaired Student's t test with Welch's correction. Shown is correlation of MIF protein levels and PLT levels in patients with MPNs; simple linear regression testing.

(B) MIF protein levels divided according to genotype (Jak2^{V617F}, n = 33; CALR^{mut}, n = 21). One-way ANOVA; *p < 0.05, **p < 0.01, ****p < 0.0001.

(C) *JAK2^{V617F}* mutant HEL cells were treated with 500 nM ruxolitinib for 24 h or 250 nM BEZ235 for 4 h, and *MIF* expression levels relative to *GAPDH* were quantified by qPCR and normalized to the DMSO-treated control (n = 3). Unpaired Student's t test with Welch's correction.

(D) C57BL/6 recipient mice received lethal irradiation followed by transplantation with either WT or *MIF*$^{-/-}$ cKit$^+$ HSPCs transduced with either ThPO or empty vector (EV) control lentiviral vectors (n = 5/group). Mice were sacrificed 32 days after transplantation. Monocytes (CD11b$^+$ GR1$^-$) and macrophages (F4/80$^+$GR1$^-$) in the PB were analyzed via FACS over the course of the experiment. Mean ± SEM, two-way ANOVA followed by Tukey's post hoc test; significance for values at sacrifice is indicated.

(E) Monocytes (CD11b$^+$ GR1$^-$) and macrophages (F4/80$^+$GR1$^-$) were analyzed in the BM at sacrifice via FACS. Mean ± SEM, one way ANOVA followed by Tukey's post hoc test.

(F) Representative images of H&E staining of the femur. Scale bar, 60 μm.

(G) Representative images of reticulin staining. Scale bar, 200 μm.

(H) Quantification of myelofibrosis grade based on reticulin staining of the femur.

(I) BM cellularity (total cell count) and viability (percent trypan blue negative) at sacrifice.

(J) Human BM-MSC cell line cultured with conditioned medium collected from spin embryoid bodies (EBs) generated from either *JAK2^{WT}* or *JAK2^{V617F}* patient-derived IPSCs (n = 2 each) and treated with 40 μM ISO-1 or DMSO for 48 h. Col1a1 expression was quantified with qPCR relative to HPRT1, normalized to respective JAK2^{WT} conditioned medium, untreated conditions (n = 3).

Mean ± SEM, one-way ANOVA followed by Tukey's post hoc test. *p < 0.05, **p < 0.01, ***p < 0.001, ****p < 0.0001. See also Figure S5.

not fully consider the potential role of non-canonical Hh signaling. Additionally, without transplantation into Gli1-competent mice, analysis of the hematopoietic compartment in steady-state Gli1-null mice cannot rule out the contribution of non-hematopoietic cell types to observed phenotypes. By using Gli1, Gli2, or SMO knockout mice as donors and transplanting into WT, Hh signaling competent recipients, we here systematically deciphered the role of hematopoietic canonical and non-canonical Hh signaling in normal hematopoiesis and in MPNs.

Inhibition of the canonical Gli protein activator SMO has been proven to be an effective treatment in some cancer types[11] and is FDA approved for BCC. Similar attempts to target it in MPNs has had varied success.[12] In line, our data show that the genetic knockout of *Smo* is insufficient to reduce disease progression. Two MPN-relevant cytokines, TGFb1[21,22] and IL-6,[22–24] increase in GLI1 protein levels in PBMCs from HDs, showing that GLI1 activation can occur in a non-canonical fashion in MPNs and that it can be propagated to non-mutated cells by the inflammatory environment caused by the mutant hematopoietic clone. Knockout of *Gli2* was unable to rescue the MPN phenotype or ameliorate fibrosis, pointing to a specific role of *Gli1* rather than general activation of the Hh pathway. Recent studies using *Gli1*$^{-/-}$ mice indicate a specific role of *Gli1* in regulation of HSPC function and cycling. *Gli1*$^{-/-}$ mice exhibit increased numbers of LT HSCs and increased engraftment in competitive transplantation studies,[55] in line with our findings that the absence of *Gli1* does not have any detrimental effects on normal HSPCs.

Our data show that hematopoietic *Gli1* is crucial for malignant hematopoietic-stromal cell crosstalk in MPNs and affects key pathways in the disease pathogenesis. A key hallmark of MPNs and PMF is inflammation.[56–58] Proinflammatory cytokines, such as TNF-α, are linked to the survival of the *Jak2*^{V617F} malignant clone[59] and to stromal cell activation in fibrosis.[26] Our data show that TNF-α signaling via nuclear factor κB (NF-κB) is significantly downregulated when hematopoietic *Gli1* is inhibited in MPNs. Additionally, stromal cells under this condition also show the same pattern of downregulation, indicating a role of *Gli1* in the communication of this signal between cell types.

PI3K/AKT signaling is important in PMF because it is critical for *Jak2*^{V617F}-mediated cellular dysregulation.[60] Our data show that inhibition of hematopoietic *Gli1* reduces upregulation of this pathway in both hematopoietic and stromal cells. Given that the PI3K/AKT pathway has been shown previously to both activate *Gli1* in a noncanonical fashion[46] and also be activated itself by *Gli1*,[45] this is one mechanism by which *Gli1* signaling is perpetuated and transmitted between cell types in MPNs, in particular because the application of a PI3K inhibitor inhibited the fibrotic transformation of fibrosis-driving cells.

The *Gli1*-MIF/CD74 axis is relevant in this context because it also both activates and is regulated by the PI3K/AKT pathway[61,62] and is linked to inflammation[63,64] and fibrosis.[65,66] MIF is interesting to be followed up on as a diagnostic marker because it is a secreted factor, and protein levels in serum of patients show a significant association with MPNs. We have shown that genetically inhibiting hematopoietic MIF reduces fibrotic transformation *in vivo* in a murine MPN model and that the MIF/CD74 axis is druggable. We thus conclude that targeting MIF in MPNs would interrupt crucial hematopoietic-stromal, pro-fibrotic crosstalk. Our data also indicate the application of combinatorial strategies by pointing out a JAK2^{V617F}-PI3K-GLI1-MIF-CD74 axis that exerts cell-intrinsic and -extrinsic effects on the MPN clone and the fibrotic transformation.

Activation of GLI1 can occur independent of canonical Hh signaling and is directly associated with the JAK2^{V617F} mutation in MPN. Therefore, specific, direct targeting of this TF is needed rather than inhibiting upstream nodes of the Hh pathway. Downstream of GLI1 in MPNs, multiple pathways and genes are activated and upregulated, including PI3K and MIF; the complex paracrine and autocrine interactions between these nodes result in increased secretion of MIF, which, in turn, increases expression of fibrosis-relevant genes in stromal cells. Our data highlight the importance of combinatorial strategies to interrupt pro-fibrotic intracellular signaling and intercellular crosstalk, which might be more effective than either alone.

Limitations of the study

Our findings of increased GLI1 protein levels in hematopoietic cells were only from patients with MPNs harboring a JAK2^{V617F} mutation; thus, larger cohorts with varied mutational statuses and more controls are needed. The kinetics of the disease might also play a role because GLI1 knockout had more effect in the JAK2^{V617F} model, which has slower kinetics of disease progression than ThPO overexpression. We acknowledge that GLI2 and SMO are floxed, conditional genetic knockout models needing poly(I:C) for excision, while the GLI1 model is a germline, non-inducible knockout. All experiments had a respective control cohort, and while we waited an appropriate amount of time prior to transplanting to ensure that any cycling effects on the HSPCs were mitigated, only the inducible knockout lines and their controls received poly(I:C), which may be a confounder. The frequency of GFP^{+} cells showed variability in the mice that was not reflected in the phenotype. In our scRNA-seq, a higher number of stromal cells might increase insights into GLI1-mediated crosstalk. Although our data link PI3K with GLI1 in MPNs, and we saw an effect of PI3K inhibition on the fibrotic transformation of stromal cells, clinical trials of inhibitors targeting this pathway were halted due to insufficient improvement.

STAR★METHODS

Detailed methods are provided in the online version of this paper and include the following:

- KEY RESOURCES TABLE
- RESOURCE AVAILABILITY
  - Lead contact
  - Materials availability
  - Data and code availability
- EXPERIMENTAL MODEL AND STUDY PARTICIPANT DETAILS
  - Human studies
  - Mouse studies
- METHOD DETAILS
  - Patient samples
  - Mouse experiments

- ○ Viral transduction
- ○ Flow cytometry
- ○ Stimulation of HD PBMCs
- ○ Human megakaryocytic cell line culture
- ○ Patient-derived IPSC lines and JAK2 conditioned medium
- ○ Murine hematopoietic progenitor cell lines and ThPO conditioned medium
- ○ Generation of hMSC cell line, subsequent recombinant cytokine and conditioned medium stimulation
- ○ Isolation of primary murine MSCs and subsequent stimulation with ThPO conditioned medium
- ○ Culture and treatment of HEL cell line
- ○ Culture and stimulation of MSOD cell line
- ○ Histological staining
- ○ scRNA sequencing sample preparation
- ○ scRNA library preparation and sequencing
- ○ scRNA-seq data—Alignment
- ○ scRNA-seq data—Initial processing
- ○ scRNA-seq data—Cluster annotation
- ○ scRNA-seq data—Transcription factor analysis
- ○ scRNA-seq data—Pathway activity analysis
- ○ scRNA-seq data—Ligand-receptor analysis
- ○ RNA isolation and RT-qPCR analysis
- ○ Primer sequences
- ○ ELISA

- ● QUANTIFICATION AND STATISTICAL ANALYSIS
  - ○ Image processing and quantification
  - ○ Statistical analysis

SUPPLEMENTAL INFORMATION

Supplemental information can be found online at https://doi.org/10.1016/j.celrep.2023.113608.

ACKNOWLEDGMENTS

R.K.S. is an Oncode investigator, was supported by a KWF Kankerbestrijding grant (11031/2017-1, Bas Mulder Award, Dutch Cancer Foundation) and an ERC grant (deFIBER, ERC-StG 757339), and has support through the Network CANcer TARgeting (CANTAR) funded by the Ministerium für Kultur und Wissenschaft des Landes Nordrhein-Westfalen. This work was supported by grants of the Deutsche Forschungsgemeinschaft (DFG) (KR 4073/9-1to R.K., SCHN1188/6-1to R.K.S., KO2155/7-1to S.K., CH1501/1-1to N.C., GL1093/1-2 to H.G., and GE2811/4-1to I.C.) within the clinical research unit CRU344. This work was in part supported by NCI 2P30CA008748-48 (MSK Cancer Center support grant) and NCI P01-CA108671. R.K., I.G.C., and R.K.S. are members of the E:MED Consortium Fibromap funded by the German Ministry of Education and Science (BMBF). We thank Ivan Martin for kindly providing the MSOD cells and Jürgen Bernhagen for providing the MIF and CD74 knockout mouse lines.

AUTHOR CONTRIBUTIONS

J.E. Pritchard designed and carried out experiments, analyzed and interpreted data, performed biocomputational analyses, and wrote the manuscript. J.E. Pearce, J.S.N., V.K., R.S., O.N., and M.T.H., performed biocomputational analyses, interpreted the results, and reviewed the manuscript. I.A.M.S., S.N.R.F., K.G., F.P., S.W., A.B., N.L., A.K.G., E.S., B.B., N.F., K.B., E.B., K.O., and H.F.E.G. performed experiments, analyzed and interpreted data, and reviewed the manuscript. S.K., N.C., M.B., N.B., A.D., and R.L.L. selected patient specimens, performed experiments, shared antibodies and cells, and reviewed the manuscript. I.G.C. and R.K. critically discussed the data, shared materials, analyzed and interpreted data, and reviewed the manuscript. R.K.S. obtained funding, designed and carried out experiments, analyzed data, and wrote the manuscript. All authors provided critical analysis of the manuscript.

DECLARATION OF INTERESTS

N.B. is employed by Prelude Therapeutics. S.K. received research grants from Geron, Janssen, AOP Pharma, and Novartis; received consulting fees from Pfizer, Incyte, Ariad, Novartis, AOP Pharma, Bristol Myers Squibb, Celgene, Geron, Janssen, CTI BioPharma, Roche, Bayer, PharmaEssentia, Sierra Oncology, Imago Biosciences, and GSK; payment or honoraria from Novartis, BMS/Celgene, and Pfizer; received travel/accommodation support from Alexion, Novartis, Bristol Myers Squibb, Incyte, AOP Pharma, CTI BioPharma, Pfizer, Celgene, Janssen, Geron, Roche, AbbVie, Sierra Oncology, and Karthos; and participated on advisory boards for Pfizer, Incyte, Ariad, Novartis, AOP Pharma, BMS, Celgene, Geron, Janssen, CTI BioPharma, Roche, Bayer, Sierra Oncology, PharmaEssentia, Imago Biosciences, and GSK. R.L.L. is on the supervisory board of QIAGEN and is a scientific advisor to Imago, Mission Bio, Zentalis, Ajax, Auron, Prelude, C4 Therapeutics, and Isoplexis; receives research support from Ajax, Zentalis, and Abbvie; consulted for Incyte, Janssen, and Astra Zeneca; and received honoraria from Astra Zeneca for invited lectures. R.K. has grants from Travere Therapeutics, Galapagos, Chugai, and Novo Nordisk and is a consultant for Bayer, Pfizer, Novo Nordisk, and Gruenenthal. I.G.C. has a grant from Illumina. R.K. and R.K.S. are founders and shareholders of Sequantrix GmbH. N.F. is employed by Sequantrix GmbH.

Received: March 1, 2023
Revised: September 28, 2023
Accepted: December 6, 2023
Published: December 20, 2023

REFERENCES

1. Baxter, E.J., Scott, L.M., Campbell, P.J., East, C., Fourouclas, N., Swanton, S., Vassiliou, G.S., Bench, A.J., Boyd, E.M., Curtin, N., et al. (2005). Acquired mutation of the tyrosine kinase JAK2 in human myeloproliferative disorders. Lancet *365*, 1054–1061.
2. Vainchenker, W., Delhommeau, F., Constantinescu, S.N., and Bernard, O.A. (2011). New mutations and pathogenesis of myeloproliferative neoplasms. Blood *118*, 1723–1735.
3. Rampal, R., Al-Shahrour, F., Abdel-Wahab, O., Patel, J.P., Brunel, J.P., Mermel, C.H., Bass, A.J., Pretz, J., Ahn, J., Hricik, T., et al. (2014). Integrated genomic analysis illustrates the central role of JAK-STAT pathway activation in myeloproliferative neoplasm pathogenesis. Blood *123*, e123–e133.
4. Thorsten, K., Gisslinger, H., Harutyunyan, A.S., Nivarthi, H., Rumi, E., Milosevic, J.D., Them, N.C.C., Berg, T., Gisslinger, B., Pietra, D., et al. (2013). Frequent Mutations in the Calreticulin Gene CALR in Myeloproliferative Neoplasms. Blood *122*.
5. Schneider, R.K., Mullally, A., Dugourd, A., Peisker, F., Hoogenboezem, R., Van Strien, P.M.H., Bindels, E.M., Heckl, D., Büsche, G., Fleck, D., et al. (2017). Gli1(+) Mesenchymal Stromal Cells Are a Key Driver of Bone Marrow Fibrosis and an Important Cellular Therapeutic Target. Cell Stem Cell *20*, 785–800.e8.
6. Kramann, R., Schneider, R.K., DiRocco, D.P., Machado, F., Fleig, S., Bondzie, P.A., Henderson, J.M., Ebert, B.L., and Humphreys, B.D. (2015). Perivascular Gli1+ progenitors are key contributors to injury-induced organ fibrosis. Cell Stem Cell *16*, 51–66.
7. Cassandras, M., Wang, C., Kathiriya, J., Tsukui, T., Matatia, P., Matthay, M., Wolters, P., Molofsky, A., Sheppard, D., Chapman, H., and Peng, T. (2020). Gli1(+) mesenchymal stromal cells form a pathological niche to promote airway progenitor metaplasia in the fibrotic lung. Nat. Cell Biol. *22*, 1295–1306.

8. Wu, S.M., Choo, A.B.H., Yap, M.G.S., and Chan, K.K.K. (2010). Role of Sonic hedgehog signaling and the expression of its components in human embryonic stem cells. Stem Cell Res. *4*, 38–49.
9. Skoda, A.M., Simovic, D., Karin, V., Kardum, V., Vranic, S., and Serman, L. (2018). The role of the Hedgehog signaling pathway in cancer: A comprehensive review. Bosn. J. Basic Med. Sci. *18*, 8–20.
10. Klein, C., Zwick, A., Kissel, S., Forster, C.U., Pfeifer, D., Follo, M., Illert, A.L., Decker, S., Benkler, T., Pahl, H., et al. (2016). Ptch2 loss drives myeloproliferation and myeloproliferative neoplasm progression. J. Exp. Med. *213*, 273–290.
11. Li, Y., Song, Q., and Day, B.W. (2019). Phase I and phase II sonidegib and vismodegib clinical trials for the treatment of paediatric and adult MB patients: a systemic review and meta-analysis. Acta Neuropathol. Commun. *7*, 123.
12. Sasaki, K., Gotlib, J.R., Mesa, R.A., Newberry, K.J., Ravandi, F., Cortes, J.E., Kelly, P., Kutok, J.L., Kantarjian, H.M., and Verstovsek, S. (2015). Phase II evaluation of IPI-926, an oral Hedgehog inhibitor, in patients with myelofibrosis. Leuk. Lymphoma *56*, 2092–2097.
13. Gerds, A.T., Tauchi, T., Ritchie, E., Deininger, M., Jamieson, C., Mesa, R., Heaney, M., Komatsu, N., Minami, H., Su, Y., et al. (2019). Phase 1/2 trial of glasdegib in patients with primary or secondary myelofibrosis previously treated with ruxolitinib. Leuk. Res. *79*, 38–44.
14. Gupta, V., Wolleschak, D., Hasselbalch, H., Vannucchi, A.M., Koschmieder, S., Cervantes, F., Li, Y., Dong, T., Wroclawska, M., Bharathy, S., and Harrison, C. (2020). Safety and efficacy of the combination of sonidegib and ruxolitinib in myelofibrosis: a phase 1b/2 dose-finding study. Blood Adv. *4*, 3063–3071.
15. Couban, S., Benevolo, G., Donnellan, W., Cultrera, J., Koschmieder, S., Verstovsek, S., Hooper, G., Hertig, C., Tandon, M., Dimier, N., et al. (2018). A phase Ib study to assess the efficacy and safety of vismodegib in combination with ruxolitinib in patients with intermediate- or high-risk myelofibrosis. J. Hematol. Oncol. *11*, 122.
16. Hofmann, I., Stover, E.H., Cullen, D.E., Mao, J., Morgan, K.J., Lee, B.H., Kharas, M.G., Miller, P.G., Cornejo, M.G., Okabe, R., et al. (2009). Hedgehog signaling is dispensable for adult murine hematopoietic stem cell function and hematopoiesis. Cell Stem Cell *4*, 559–567.
17. Gao, J., Graves, S., Koch, U., Liu, S., Jankovic, V., Buonamici, S., El Andaloussi, A., Nimer, S.D., Kee, B.L., Taichman, R., et al. (2009). Hedgehog signaling is dispensable for adult hematopoietic stem cell function. Cell Stem Cell *4*, 548–558.
18. Bhagwat, N., Keller, M.D., Rampal, R.K., Shank, K., de Stanchina, E., Rose, K., Amakye, D., and Levine, R.L. (2013). Improved Efficacy Of Combination Of JAK2 and Hedgehog Inhibitors In Myelofibrosis. Blood *122*, 666.
19. Lim, K.H., Chen, C.G.S., Chang, Y.C., Chiang, Y.H., Kao, C.W., Wang, W.T., Chang, C.Y., Huang, L., Lin, C.S., Cheng, C.C., et al. (2017). Increased B cell activation is present in JAK2V617F-mutated, CALR-mutated and triple-negative essential thrombocythemia. Oncotarget *8*, 32476–32491.
20. Cervantes, F., Hernández-Boluda, J.C., Villamor, N., Serra, A., and Montserrat, E. (2000). Assessment of peripheral blood lymphocyte subsets in idiopathic myelofibrosis. Eur. J. Haematol. *65*, 104–108.
21. Wong, W.J., Baltay, M., Getz, A., Fuhrman, K., Aster, J.C., Hasserjian, R.P., and Pozdnyakova, O. (2019). Gene expression profiling distinguishes prefibrotic from overtly fibrotic myeloproliferative neoplasms and identifies disease subsets with distinct inflammatory signatures. PLoS One *14*, e0216810.
22. Jutzi, J.S., and Mullally, A. (2020). Remodeling the Bone Marrow Microenvironment – A Proposal for Targeting Pro-inflammatory Contributors in MPN. Front. Immunol. *11*, 2093.
23. Cacemiro, M.D.C., Cominal, J.G., Tognon, R., Nunes, N.d.S., Simões, B.P., Figueiredo-Pontes, L.L.d., Catto, L.F.B., Traina, F., Souto, E.X., Zambuzi, F.A., et al. (2018). Philadelphia-negative myeloproliferative neoplasms as disorders marked by cytokine modulation. Hematol. Transfus. Cell Ther. *40*, 120–131.
24. Hsu, H.C., Tsai, W.H., Jiang, M.L., Ho, C.H., Hsu, M.L., Ho, C.K., and Wang, S.Y. (1999). Circulating levels of thrombopoietic and inflammatory cytokines in patients with clonal and reactive thrombocytosis. J. Lab. Clin. Med. *134*, 392–397.
25. Gleitz, H.F.E., Dugourd, A.J.F., Leimkühler, N.B., Snoeren, I.A.M., Fuchs, S.N.R., Menzel, S., Ziegler, S., Kröger, N., Triviai, I., Büsche, G., et al. (2020). Increased CXCL4 expression in hematopoietic cells links inflammation and progression of bone marrow fibrosis in MPN. Blood *136*, 2051–2064.
26. Leimkühler, N.B., Gleitz, H.F.E., Ronghui, L., Snoeren, I.A.M., Fuchs, S.N.R., Nagai, J.S., Banjanin, B., Lam, K.H., Vogl, T., Kuppe, C., et al. (2021). Heterogeneous bone-marrow stromal progenitors drive myelofibrosis via a druggable alarmin axis. Cell Stem Cell *28*, 637–652.e638.
27. Kramann, R., Fleig, S.V., Schneider, R.K., Fabian, S.L., DiRocco, D.P., Maarouf, O., Wongboonsin, J., Ikeda, Y., Heckl, D., Chang, S.L., et al. (2015). Pharmacological GLI2 inhibition prevents myofibroblast cell-cycle progression and reduces kidney fibrosis. J. Clin. Invest. *125*, 2935–2951.
28. Zhang, X., Lan, Y., Xu, J., Quan, F., Zhao, E., Deng, C., Luo, T., Xu, L., Liao, G., Yan, M., et al. (2019). CellMarker: a manually curated resource of cell markers in human and mouse. Nucleic Acids Res. *47*, D721–D728.
29. Stalmann, U.S.A., Banjanin, B., Snoeren, I.A.M., Nagai, J.S., Leimkühler, N.B., Li, R., Benabid, A., Pritchard, J.E., Malyaran, H., Neuss, S., et al. (2022). Single-cell analysis of cultured bone marrow stromal cells reveals high similarity to fibroblasts in situ. Exp. Hematol. *110*, 28–33.
30. Liao, Y., Wang, J., Jaehnig, E.J., Shi, Z., and Zhang, B. (2019). WebGestalt 2019: gene set analysis toolkit with revamped UIs and APIs. Nucleic Acids Res. *47*, W199–W205.
31. Baccin, C., Al-Sabah, J., Velten, L., Helbling, P.M., Grünschläger, F., Hernández-Malmierca, P., Nombela-Arrieta, C., Steinmetz, L.M., Trumpp, A., and Haas, S. (2020). Combined single-cell and spatial transcriptomics reveal the molecular, cellular and spatial bone marrow niche organization. Nat. Cell Biol. *22*, 38–48.
32. Meng, M., Sang, L., and Wang, X. (2019). S100 Calcium Binding Protein A11 (S100A11) Promotes The Proliferation, Migration And Invasion Of Cervical Cancer Cells, And Activates Wnt/β-Catenin Signaling. OncoTargets Ther. *12*, 8675–8685.
33. Navrátilová, A., Bečvář, V., Baloun, J., Damgaard, D., Nielsen, C.H., Veigl, D., Pavelka, K., Vencovský, J., Šenolt, L., and Andrés Cerezo, L. (2021). S100A11 (calgizzarin) is released via NETosis in rheumatoid arthritis (RA) and stimulates IL-6 and TNF secretion by neutrophils. Sci. Rep. *11*, 6063.
34. Lucijanic, M., Livun, A., Tomasovic-Loncaric, C., Stoos-Veic, T., Pejsa, V., Jaksic, O., Prka, Z., and Kusec, R. (2016). Canonical Wnt/β-Catenin Signaling Pathway Is Dysregulated in Patients With Primary and Secondary Myelofibrosis. Clin. Lymphoma, Myeloma & Leukemia *16*, 523–526.
35. Balliu, M., Calabresi, L., Bartalucci, N., Romagnoli, S., Maggi, L., Manfredini, R., Lulli, M., Guglielmelli, P., and Vannucchi, A.M. (2021). Activated IL-6 signaling contributes to the pathogenesis of, and is a novel therapeutic target for, CALR-mutated MPNs. Blood Adv. *5*, 2184–2195.
36. Zheng, Y., Miyamoto, D.T., Wittner, B.S., Sullivan, J.P., Aceto, N., Jordan, N.V., Yu, M., Karabacak, N.M., Comaills, V., Morris, R., et al. (2017). Expression of β-globin by cancer cells promotes cell survival during blood-borne dissemination. Nat. Commun. *8*, 14344.
37. Mondet, J., Hussein, K., and Mossuz, P. (2015). Circulating Cytokine Levels as Markers of Inflammation in Philadelphia Negative Myeloproliferative Neoplasms: Diagnostic and Prognostic Interest. Mediat. Inflamm. *2015*, 670580.
38. Leiva, O., Ng, S.K., Chitalia, S., Balduini, A., Matsuura, S., and Ravid, K. (2017). The role of the extracellular matrix in primary myelofibrosis. Blood Cancer J. *7*, e525.
39. Li, R., Colombo, M., Wang, G., Rodriguez-Romera, A., O'Sullivan, J., Clark, S.-A., Sáez, J.M.P., Meng, Y., Khan, A.O., Wen, S., et al. (2023). A

pro-inflammatory stem cell niche drives myelofibrosis through a targetable galectin 1 axis. Preprint at bioRxiv.

40. Barsoum, I., and Yao, H.H.C. (2011). Redundant and differential roles of transcription factors Gli1 and Gli2 in the development of mouse fetal Leydig cells. Biol. Reprod. *84*, 894–899.

41. Garcia-Alonso, L., Holland, C.H., Ibrahim, M.M., Turei, D., and Saez-Rodriguez, J. (2019). Benchmark and integration of resources for the estimation of human transcription factor activities. Genome Res. *29*, 1363–1375.

42. Liberzon, A., Birger, C., Thorvaldsdóttir, H., Ghandi, M., Mesirov, J.P., and Tamayo, P. (2015). The Molecular Signatures Database (MSigDB) hallmark gene set collection. Cell Syst. *1*, 417–425.

43. Van Egeren, D., Escabi, J., Nguyen, M., Liu, S., Reilly, C.R., Patel, S., Kamaz, B., Kalyva, M., DeAngelo, D.J., Galinsky, I., et al. (2021). Reconstructing the Lineage Histories and Differentiation Trajectories of Individual Cancer Cells in Myeloproliferative Neoplasms. Cell Stem Cell *28*, 514–523.e9.

44. Larsen, T.S., Christensen, J.H., Hasselbalch, H.C., and Pallisgaard, N. (2007). The JAK2 V617F mutation involves B- and T-lymphocyte lineages in a subgroup of patients with Philadelphia-chromosome negative chronic myeloproliferative disorders. Br. J. Haematol. *136*, 745–751.

45. Zhou, C., Du, J., Zhao, L., Liu, W., Zhao, T., Liang, H., Fang, P., Zhang, K., and Zeng, H. (2021). GLI1 reduces drug sensitivity by regulating cell cycle through PI3K/AKT/GSK3/CDK pathway in acute myeloid leukemia. Cell Death Dis. *12*, 231.

46. Zhou, J., Zhu, G., Huang, J., Li, L., Du, Y., Gao, Y., Wu, D., Wang, X., Hsieh, J.-T., He, D., and Wu, K. (2016). Non-canonical GLI1/2 activation by PI3K/AKT signaling in renal cell carcinoma: A novel potential therapeutic target. Cancer Lett. *370*, 313–323.

47. Darby, I.A., and Hewitson, T.D. (2016). Hypoxia in tissue repair and fibrosis. Cell Tissue Res. *365*, 553–562.

48. Tratwal, J., Bekri, D., Boussema, C., Sarkis, R., Kunz, N., Koliqi, T., Rojas-Sutterlin, S., Schyrr, F., Tavakol, D.N., Campos, V., et al. (2020). MarrowQuant Across Aging and Aplasia: A Digital Pathology Workflow for Quantification of Bone Marrow Compartments in Histological Sections. Front. Endocrinol. *11*, 480.

49. Yacoub, A., Borate, U., Rampal, R., Ali, H., Wang, E., Gerds, A., Hobbs, G., Kremyanskaya, M., Winton, E., O'Connell, C., et al. (2022). MPN-075 Efficacy and Safety of Add-on Parsaclisib to Ruxolitinib Therapy in Myelofibrosis Patients With Low Versus Higher Baseline Platelet Counts: A Subgroup Analysis of Data From a Phase 2 Study. Clin. Lymphoma, Myeloma & Leukemia *22* (*Suppl 2*), S324.

50. Yacoub, A., Borate, U., Rampal, R., Ali, H., Wang, E.S., Gerds, A.T., Hobbs, G., Kremyanskaya, M., Winton, E., O'Connell, C., et al. (2021). Subgroup Analysis from a Phase 2 Study of the Efficacy and Safety of Parsaclisib, a Selective PI3Kδ Inhibitor, in Combination with Ruxolitinib in Patients with Myelofibrosis (MF). Blood *138*, 3647.

51. Dibble, C.C., and Cantley, L.C. (2015). Regulation of mTORC1 by PI3K signaling. Trends Cell Biol. *25*, 545–555.

52. Kramann, R., and Schneider, R.K. (2018). The identification of fibrosis-driving myofibroblast precursors reveals new therapeutic avenues in myelofibrosis. Blood *131*, 2111–2119.

53. Nagai, J.S., Leimkühler, N.B., Schaub, M.T., Schneider, R.K., and Costa, I.G. (2021). CrossTalkeR: analysis and visualization of ligand-receptorne tworks. Bioinformatics *37*, 4263–4265.

54. Fiskus, W., Verstovsek, S., Manshouri, T., Smith, J.E., Peth, K., Abhyankar, S., McGuirk, J., and Bhalla, K.N. (2013). Dual PI3K/AKT/mTOR inhibitor BEZ235 synergistically enhances the activity of JAK2 inhibitor against cultured and primary human myeloproliferative neoplasm cells. Mol. Cancer Therapeut. *12*, 577–588.

55. Merchant, A., Joseph, G., Wang, Q., Brennan, S., and Matsui, W. (2010). Gli1 regulates the proliferation and differentiation of HSCs and myeloid progenitors. Blood *115*, 2391–2396.

56. Gleitz, H.F.E., Benabid, A., and Schneider, R.K. (2021). Still a burning question: the interplay between inflammation and fibrosis in myeloproliferative neoplasms. Curr. Opin. Hematol. *28*, 364–371.

57. Mendez Luque, L.F., Blackmon, A.L., Ramanathan, G., and Fleischman, A.G. (2019). Key Role of Inflammation in Myeloproliferative Neoplasms: Instigator of Disease Initiation, Progression. and Symptoms. Curr. Hematol. Malig. Rep. *14*, 145–153.

58. Hasselbalch, H.C., and Bjørn, M.E. (2015). MPNs as Inflammatory Diseases: The Evidence, Consequences, and Perspectives. Mediat. Inflamm. *2015*, 102476.

59. Fleischman, A.G., Aichberger, K.J., Luty, S.B., Bumm, T.G., Petersen, C.L., Doratotaj, S., Vasudevan, K.B., LaTocha, D.H., Yang, F., Press, R.D., et al. (2011). TNFα facilitates clonal expansion of JAK2V617F positive cells in myeloproliferative neoplasms. Blood *118*, 6392–6398.

60. Kamishimoto, J., Tago, K., Kasahara, T., and Funakoshi-Tago, M. (2011). Akt activation through the phosphorylation of erythropoietin receptor at tyrosine 479 is required for myeloproliferative disorder-associated JAK2 V617F mutant-induced cellular transformation. Cell. Signal. *23*, 849–856.

61. Lue, H., Thiele, M., Franz, J., Dahl, E., Speckgens, S., Leng, L., Fingerle-Rowson, G., Bucala, R., Lüscher, B., and Bernhagen, J. (2007). Macrophage migration inhibitory factor (MIF) promotes cell survival by activation of the Akt pathway and role for CSN5/JAB1 in the control of autocrine MIF activity. Oncogene *26*, 5046–5059.

62. Oliveira, C.S., de Bock, C.E., Molloy, T.J., Sadeqzadeh, E., Geng, X.Y., Hersey, P., Zhang, X.D., and Thorne, R.F. (2014). Macrophage migration inhibitory factor engages PI3K/Akt signalling and is a prognostic factor in metastatic melanoma. BMC Cancer *14*, 630.

63. Mitchell, R.A., Liao, H., Chesney, J., Fingerle-Rowson, G., Baugh, J., David, J., and Bucala, R. (2002). Macrophage migration inhibitory factor (MIF) sustains macrophage proinflammatory function by inhibiting p53: regulatory role in the innate immune response. Proc. Natl. Acad. Sci. USA *99*, 345–350.

64. Donn, R.P., and Ray, D.W. (2004). Macrophage migration inhibitory factor: molecular, cellular and genetic aspects of a key neuroendocrine molecule. J. Endocrinol. *182*, 1–9.

65. Luo, Y., Yi, H., Huang, X., Lin, G., Kuang, Y., Guo, Y., and Xie, C. (2021). Inhibition of macrophage migration inhibitory factor (MIF) as a therapeutic target in bleomycin-induced pulmonary fibrosis rats. Am. J. Physiol. Lung Cell Mol. Physiol. *321*. L6-l16.

66. Günther, S., Bordenave, J., Hua-Huy, T., Nicco, C., Cumont, A., Thuillet, R., Tu, L., Quatremarre, T., Guilbert, T., Jalce, G., et al. (2018). Macrophage Migration Inhibitory Factor (MIF) Inhibition in a Murine Model of Bleomycin-Induced Pulmonary Fibrosis. Int. J. Mol. Sci. *19*, 4105.

67. Bourgine, P., Le Magnen, C., Pigeot, S., Geurts, J., Scherberich, A., and Martin, I. (2014). Combination of immortalization and inducible death strategies to generate a human mesenchymal stromal cell line with controlled survival. Stem Cell Res. *12*, 584–598.

68. Fingerle-Rowson, G., Petrenko, O., Metz, C.N., Forsthuber, T.G., Mitchell, R., Huss, R., Moll, U., Müller, W., and Bucala, R. (2003). The p53-dependent effects of macrophage migration inhibitory factor revealed by gene targeting. Proc. Natl. Acad. Sci. USA *100*, 9354–9359.

69. Shachar, I., and Flavell, R.A. (1996). Requirement for invariant chain in B cell maturation and function. Science *274*, 106–108.

70. Stewart, S.A., Dykxhoorn, D.M., Palliser, D., Mizuno, H., Yu, E.Y., An, D.S., Sabatini, D.M., Chen, I.S.Y., Hahn, W.C., Sharp, P.A., et al. (2003). Lentivirus-delivered stable gene silencing by RNAi in primary cells. Rna *9*, 493–501.

71. Hahn, W.C., Dessain, S.K., Brooks, M.W., King, J.E., Elenbaas, B., Sabatini, D.M., DeCaprio, J.A., and Weinberg, R.A. (2002). Enumeration of the simian virus 40 early region elements necessary for human cell transformation. Mol. Cell Biol. *22*, 2111–2123.

72. Counter, C.M., Hahn, W.C., Wei, W., Caddle, S.D., Beijersbergen, R.L., Lansdorp, P.M., Sedivy, J.M., and Weinberg, R.A. (1998). Dissociation

among in vitro telomerase activity, telomere maintenance, and cellular immortalization. Proc. Natl. Acad. Sci. USA *95*, 14723–14728.

73. Hao, Y., Hao, S., Andersen-Nissen, E., Mauck, W.M., Zheng, S., Butler, A., Lee, M.J., Wilk, A.J., Darby, C., Zager, M., et al. (2021). Integrated analysis of multimodal single-cell data. Cell *184*, 3573–3587.e29.
74. Young, M.D., and Behjati, S. (2020). SoupX removes ambient RNA contamination from droplet-based single-cell RNA sequencing data. GigaScience *9*, giaa151.
75. Efremova, M., Vento-Tormo, M., Teichmann, S.A., and Vento-Tormo, R. (2020). CellPhoneDB: inferring cell–cell communication from combined expression of multi-subunit ligand–receptor complexes. Nat. Protoc. *15*, 1484–1506.
76. Yu, G., Wang, L.G., Han, Y., and He, Q.Y. (2012). clusterProfiler: an R package for comparing biological themes among gene clusters. OMICS *16*, 284–287.
77. Satoh, T., Toledo, M.A.S., Boehnke, J., Olschok, K., Flosdorf, N., Götz, K., Küstermann, C., Sontag, S., Seré, K., Koschmieder, S., et al. (2021). Human DC3 Antigen Presenting Dendritic Cells From Induced Pluripotent Stem Cells. Front. Cell Dev. Biol. *9*, 667304.
78. Vieri, M., Tharmapalan, V., Kalmer, M., Baumeister, J., Nikolić, M., Schnitker, M., Kirschner, M., Flosdorf, N., de Toledo, M.A.S., Zenke, M., et al. (2023). Cellular aging is accelerated in the malignant clone of myeloproliferative neoplasms. Blood Cancer J. *13*, 164.
79. Olschok, K., Han, L., de Toledo, M.A.S., Böhnke, J., Graßhoff, M., Costa, I.G., Theocharides, A., Maurer, A., Schüler, H.M., Buhl, E.M., et al. (2021). CALR frameshift mutations in MPN patient-derived iPSCs accelerate maturation of megakaryocytes. Stem Cell Rep. *16*, 2768–2783.
80. Liu, Y., Wang, Y., Gao, Y., Forbes, J.A., Qayyum, R., Becker, L., Cheng, L., and Wang, Z.Z. (2015). Efficient generation of megakaryocytes from human induced pluripotent stem cells using food and drug administration-approved pharmacological reagents. Stem Cells Transl. Med. *4*, 309–319.
81. Xu, H., Look, T., Prithiviraj, S., Lennartz, D., Cáceres, M.D., Götz, K., Wanek, P., Häcker, H., Kramann, R., Seré, K., and Zenke, M. (2022). CRISPR/Cas9 editing in conditionally immortalized HoxB8 cells for studying gene regulation in mouse dendritic cells. Eur. J. Immunol. *52*, 1859–1862.
82. Zhu, H., Guo, Z.-K., Jiang, X.-X., Li, H., Wang, X.-Y., Yao, H.-Y., Zhang, Y., and Mao, N. (2010). A protocol for isolation and culture of mesenchymal stem cells from mouse compact bone. Nat. Protoc. *5*, 550–560.
83. Stoeckius, M., Zheng, S., Houck-Loomis, B., Hao, S., Yeung, B.Z., Mauck, W.M., Smibert, P., and Satija, R. (2018). Cell Hashing with barcoded antibodies enables multiplexing and doublet detection for single cell genomics. Genome Biol. *19*, 224.

STAR★METHODS

KEY RESOURCES TABLE

REAGENT or RESOURCE	SOURCE	IDENTIFIER
Antibodies		
Anti-human CD19 BB700	BD	Cat #566396; RRID:AB_2744310
Anti-human CD66 b PE	BD	Cat #561650; RRID:AB_10894591
Anti-human HLA-DR PeCy7	BD	Cat #560651; RRID:AB_1727528
Anti-human CD45 APC-H7	BD	Cat #560178; RRID:AB_1645479
Anti-human CD3 BV510	BD	Cat #566779; RRID:AB_2869862
Anti-human CD88 BV786	BD	Cat #742320; RRID:AB_2740700
Anti-human CD89 BV786	BD	Cat #744379; RRID:AB_2742192
Anti-mouse CD117 micro beads	Miltenyi	Cat #130-091-224; RRID:AB_2753213
Anti-mouse Lineage cell depletion kit	Miltenyi	Cat #130-090-858
Anti-mouse CD3 PE	BioLegend	Cat #100206; RRID:AB_312663
Anti-mouse CD41 PeCy7	BioLegend	Cat #133916; RRID:AB_11124102
Anti-mouse GR1 ef450	ThermoFisher	Cat #48-5931-82; RRID:AB_1548788
Anti-mouse CD11b APC	BioLegend	Cat #101212; RRID:AB_312795
Anti-mouse CD45.1 APCCy7	BioLegend	Cat #110716; RRID:AB_313505
Anti-mouse CD45.2 PerCPCy5.5	BioLegend	Cat #109828; RRID:AB_893350
Anti-mouse CD117 (c-kit) APC	BioLegend	Cat #105812; RRID:AB_313221
Anti-mouse Sca1 PerCPCy5.5	BioLegend	Cat #122523; RRID:AB_893621
Anti-mouse CD48 APCCy7	BioLegend	Cat #103432; RRID:AB_2561463
Anti-mouse CD150 PeCy7	BioLegend	Cat #115914; RRID:AB_439797
Anti-mouse CD45.2 PE	Sony Biotech	Cat #1149040
Anti-mouse CD3 ef450	ThermoFisher	Cat #48-0032-82; RRID:AB_1272193
Anti-mouse B220 ef450	ThermoFisher	Cat #48-0452-82; RRID:AB_1548761
Anti-mouse CD11b ef450	ThermoFisher	Cat #48-0112-82; RRID:AB_1582236
Anti-mouse Ter119 ef450	ThermoFisher	Cat #48-5921-82; RRID:AB_1518808
Anti-mouse TotalSeq A0307	Biolegend	Cat #155813; RRID:AB_2750039

(*Continued on next page*)

Continued		
REAGENT or RESOURCE	SOURCE	IDENTIFIER
Anti-mouse TotalSeq A0308	Biolegend	Cat #155815; RRID:AB_2750040
Anti-mouse TotalSeq A0309	Biolegend	Cat #155817; RRID:AB_27500423
Anti-mouse Gli1 AF647	Novus Biologicals	Cat #NB600-600AF647
Bacterial and virus strains		
pRRL.PPT.SFFV.IRES2.EGFP.WPRE	Axels Schambach, Dirk Heckl	N/A
MSCV-IRES-EGFP	Tannishtha Reya	Addgene #20672
pMIG-JAK2V617F-IRES-EGFP	Melanie Curie	N/A
pMIG-JAK2WT-IRES-EGFP	Melanie Curie	N/A
Chemicals, peptides, and recombinant proteins		
PolyI:C	Invivogen	Cat #tlrl-pic-5
RetroNectin recombinant Human Fibronectin Fragment	Takara	Cat #T100B
CellGro Media	CellGenix GmbH	Cat #20802-0500
Murine Stem Cell Factor (*m*-SCF)	Preprotech	Cat #250-03
Murine Thrombopoietin (mTPO)	Preprotech	Cat #315-14
Fugene	Promega	Cat #E2691
Calciein red/orange	ThermoFisher	Cat #C34851
HyClone AlphaMEM	Cytiva	Cat #SH30265.01
Sodium Pyruvate	Gibco	Cat #11360070
HEPES	Gibco	Cat #15630080
Sodium Pyruvate	Gibco	Cat #11360070
Apitosilib	MedChemExpress	Cat #HY-13246
Recombinant Human TGF-b1	Invivogen	Cat #rcyc-htgfb1
Polybrene	Millipore	Cat #TR-1003-G
DMSO	Sigma	Cat #D8418
Hematoxylin Solution, Gill No.1	Sigma	Cat #GHS1128
Human SCF	Peprotech	Cat #300-07
Human IL3	Peprotech	Cat #200-03
Human IL6	Peprotech	Cat #200-06
Human Flt3L	Peprotech	Cat #300-19
RPMI	Gibco	Cat #31870074
Accutase	PAN-Biotech	Cat #P10-21500
BMP4	Miltenyi Biotec	Cat #130-111-165
Human basic FGF	Peprotech	Cat #100-18B-250
Y27632	Abcam	Cat #AB120129
L-Ascorbic Acid	Stemcell Technologies	Cat #72132
Holo-transferrin	Sigma	Cat #T0665
IMDM	Gibco	Cat #12440046
Ham's F-12 Nutrient Mix	Gibco	Cat #11765054
Chemically defined lipid concentrate	Gibco	Cat #11905031
GlutaMAX	Gibco	Cat #35050038
1-thioglycerol	Sigma	Cat #M1753
Human VEGF-C	Peprotech	Cat #100-20
hTPO	Miltenyi Biotec	Cat #130094013
ISO-1	EMD Millipore	Cat #5.05225.0001
BEZ235	Selleckchem	Cat #S1009

(*Continued on next page*)

Continued		
REAGENT or RESOURCE	SOURCE	IDENTIFIER
Ruxolitinib	Selleckchem	Cat #S1378
Trypsin	Gibco	Cat #25300054
Murine basic FGF	Peprotech	Cat #450-33
Murine EGF	Peprotech	Cat #315-09
FGF2	Peprotech	Cat #100-18C
Recombinant human MIF	Peprotech	Cat #300-69
Critical commercial assays		
Reticulin silver plating kit acc. To Gordon & Sweets	Sigma	Cat #1002510001
Sirius red fast green	Chondrex	Cat #9046
Chromium Next GEM Single Cell 3' Kit v3.1	10x Genomics	Cat #PN-1000268
Chromium Next GEM Chip G Single Cell Kit	10x Genomics	Cat #PN-1000127
Dual Index Kit TT Set A	10x Genomics	Cat #PN-1000215
NucleoSpin RNA Plus XS kit	Macherey-Nagel	Cat #740990.50
RNAeasy Mini kit	Qiagen	Cat #7401
High-Capacity cDNA Reverse Transcription Kit	Applied Biosystems	Cat #4368814
Fast SYBR Green Master Mix	Applied Biosystems	Cat #4385616
LegendMax Human Active MIF ELISA kit	BioLegend	Cat #438407
Human Sonic Hedgehog/Shh N Terminus DuoSet ELISA	R&D	Cat #DY1314-05
Transcription Factor Buffer Set	BD	Cat #562574
Deposited data		
Genome Reference Consortium Mouse Build 38 patch release 6, mm10	Genome Reference Consortium	https://www.ncbi.nlm.nih.gov/assembly/GCF_000001635.26
scRNAseq object and sample markdown	This paper	Zenodo: https://zenodo.org/doi/10.5281/zenodo.10090722
scRNAseq raw data	This paper	GEO: GSE218616
Experimental models: Cell lines		
Hek293T	ATCC	CRL-3216; RRID:CVCL_0063
hMSC cell line	This Paper	N/A
MSOD	(Bourgine et al., 2014)[67]	N/A
MEG-01	DSMZ	Cat #ACC364 RRID:CVCL_0425
SET2	DSMZ	Cat #ACC608 RRID:CVCL_2187
HEL	DSMZ	Cat #ACC11 RRID:CVCL_0001
Experimental models: Organisms/strains		
Mus musculus: Gli1tm3(re/ERT2)Alj/J	Jackson Laboratories	JAX #007913
Mus musculus: Gli2tm6Alj/J	Jackson Laboratories	JAX #007926
Mus musculus: Smotm2Amc/J	Jackson Laboratories	JAX #004526
Mus musculus: B6.Cg-Tg(Mx1-cre)1Cgn/J	Jackson Laboratories	JAX #000664
Mus musculus: C57BL/6	Jackson Laboratories	JAX #004526
Mus musculus: B6.SJL-PtprcaPepcb/BoyCrl	Charles River	#564
Mus musculus: MIF$^{-/-}$	(Fingerle-Rowson et al., 2003)[68]	N/A
Mus musculus: CD74$^{-/-}$	(Shachar and Flavell, 1996)[69]	N/A
Oligonucleotides		
See primer list in methods	See primer list in methods	See primer list in methods

(*Continued on next page*)

Continued		
REAGENT or RESOURCE	SOURCE	IDENTIFIER
Recombinant DNA		
psPAX2 (lentivral packaging)	Didier Trono	Addgene #12259
pCMV-VSV-G (lentiviral envelope)	(Stewart et al., 2003)[70]	Addgene #8454
pCL-Eco (retroviral packaging)	Novus Biologicals	Cat# NBP2-29540
pBABE-neo-largeTcDNA	(Hahn et al., 2002)[71]	Addgene #1780;
pBABE-hygro-hTERT	(Counter et al., 1998)[72]	Addgene #1773;
Software and algorithms		
GraphPad Prism v9.0.0	GraphPad Software Inc	RRID:SCR_002798
ImageJ	NIH	https://imagej.nih.gov/ij/index.html RRID:SCR_003070
R v4.0.5	CRAN	https://www.R-project.org
CellRanger v4.0.0	10x Genomics	RRID:SCR_017344
DoRothEA v1.7.2	(Garcia Alonso et al., 2019)[41]	https://github.com/saezlab/dorothea
Seurat v4.0.4	(Hao et al.,2021)[73]	https://satijalab.org/seurat/
SoupX v1.5.0	(Young et al., 2020)[74]	https://github.com/constantAmateur/SoupX
WebGestaltR v0.4.4	(Liao et al., 2019)[30]	https://github.com/bzhanglab/WebGestaltR
cellmarkersDB v1.0	(Zhang et al., 2018)[28]	http://xteam.xbio.top/CellMarker/
CellPhoneDB v2.1.7	(Efremova et al., 2020)[75]	https://github.com/Teichlab/cellphonedb
CrossTalkeR v1.3.2	(Nagai et al., 2021)[53]	https://github.com/CostaLab/CrossTalkeR
ClusterProfiler v3.18.1	(Yu et al., 2012)[76]	https://github.com/YuLab-SMU/clusterProfiler
MarrowQuant	(Tratwal et al., 2020)[48]	N/A
Adobe Photoshop CC 2023	Adobe Systems Inc.	N/A
Adobe Illustrator CC 2023	Adobe Systems Inc.	N/A
FlowJo v10.8.0	FlowJo LLC.	N/A

RESOURCE AVAILABILITY

Lead contact

Further information and requests for resources and reagents should be directed to and will be fulfilled by the lead contact, Rebekka K. Schneider, MD, PhD (reschneider@ukaachen.de).

Materials availability

This study did not generate new unique reagents. For specific details on availability please refer to the key resources table.

Data and code availability

- Single cell sequencing experiments are deposited at GEO: GSE218616. Seurat objects of dataset and sample markdown code is available at Zenodo: https://doi.org/10.5281/zenodo.10090722.
- This paper does not report original code.
- Tables with complete marker genes, differential expression, gene expression enrichment analysis, pathway and ligand receptor analysis can be found in the supplemental information of this paper.

EXPERIMENTAL MODEL AND STUDY PARTICIPANT DETAILS

Human studies

Blood samples were obtained from patients with MPN at the Department of Hematology, Oncology, Hemostaseology and Stem Cell Transplantation of RWTH Aachen University, or from fully anonymized healthy individuals at the Department of Transfusion Medicine at RWTH Aachen University, after written informed consent as approved by the Ethikkommission an der Medizinischen Fakultät der Rheinisch-Technischen Hochschule (RWTH) Aachen. (EK127/12, EK206/09 and EK099/14 respectively). Further control samples were obtained via the Institute for Clinical Chemistry at Erasmus MC, NL. Surplus material was collected from dermatological, and cardiological, orthopedic or neurological patients after diagnostics according to the ethical vote MEC-2018-1445 by the METC Erasmus Medisch Centrum Rotterdam. Additional blood samples from patients with MPN and healthy cord blood samples were collected from fully anonymized donors at Memorial Sloan Kettering Cancer Center, NY, USA according to ethical vote MSK IRB 09–141 by the Memorial Sloan Kettering Cancer Center's Institutional Review Board (IRB)/Privacy Board. Material was processed on day of acquisition. For hMSC isolation, a femur head biopsy from 66-year old orthopedic patient who underwent hip replacement, was used (ethical approval EK300-13).

All patient data was deidentified prior to inclusion. All patients provided informed consent and the data collection was performed in accordance with the Declaration of Helsinki.

Mouse studies

Mouse experiments were all approved by the Animal Welfare/Ethics committee of the EDC in accordance with legislation in the Netherlands (approval No. AVD1010020173387) Gli1tm3(re/ERT2)Alj/J (JAX Stock #007913), Gli2tm6Alj/J (JAX Stock #007926), Smotm2Amc/J (JAX Stock #004526), B6.Cg-Tg(Mx1-cre)1Cgn/J (JAX stock #003556) and C57BL/6 (JAX Stock #000664) were purchased from Jackson Laboratories (Bar Harbor, ME, USA). B6.SJL-PtprcaPepcb/BoyCrl mice were purchased from Charles River (Netherlands). MIF$^{-/-}$ mice were initially generated by Fingerle-Rowson et al.[68] and CD74$^{-/-}$ mice were initially generated by Shachar and Flavell.[69] Both MIF$^{-/-}$ and CD74$^{-/-}$ mice were kindly provided by Jürgen Bernhagen. All mice were maintained in specific-pathogen-free conditions, on a 12-h light/dark cycle and were provided with water and standard mouse chow *ad libitum*. Offspring were genotyped by PCR according to protocols provided by the Jackson Laboratories or generating labs.

METHOD DETAILS

Patient samples

Peripheral Blood mononuclear cells (PBMCs) were isolated from whole blood via density gradient (Pancoll human, PAN-Biotech) according to manufacturer's protocol. Isolated cells were frozen at -80°C in 90% FCS +10% DMSO. Serum from patients with MPN and healthy donors was isolated from whole blood, allowed to coagulate, plasma was isolated from whole blood collected in EDTA tubes. Samples were centrifuged at 2000xg for 7 min and supernatant was stored at -80°C.

Mouse experiments

In experiments using MxCre (B6.Cg-Tg(Mx1-cre)1Cgn/J), Gli2MxCre (Gli2tm6Alj/J; Tg(Mx1-cre)1Cgn) and SmoMxCre (Smotm2Amc/J; Tg(Mx1-cre)1Cgn) strains, donor mice received 3 times 200ug polyI:C (Invivogen) via intraperitoneal injection for one week, 4 weeks prior to harvesting. The Gli1tm3(re/ERT2)Alj/J line is germline knock out and therefore required no prior induction. BM from all donors (male and female) was harvested 48 h prior to transplantation and ckit^{+} enriched BM cells were transduced with ThPO lentivirus or control EV lentivirus, or Jak2^{V617F} retrovirus or control Jak2^{WT} retrovirus, depending on the model used. For all experiments, 8–10 week old B6.SJL recipient mice (female, n = 5/group) were lethally irradiated using 10.5Gy before receiving 4-5x10^{5} ckit^{+} donor cells via intravenous injection. Mice were sacrificed at 7–8 weeks post-transplant for ThPO-induced fibrosis experiments and 16–17 weeks post-transplant for Jak2^{V617F}-induced fibrosis experiments. For all analysis, comparisons were made to the respective control cohorts in each experiment.

Blood was regularly collected from the mice via submandibular bleeds into K_2EDTA coated microtainer (Becton Dickinson, NJ, USA) with full blood counts performed on a Horiba Scil Vet abc Plus hematology system.

Viral transduction

For Jak2^{V617F}/Jak2^{WT} retroviral and ThPO/EV lentiviral transduction, BM cells from 12 to 20 week-old donor mice were isolated by crushing compact bones. Cells were magnetically enriched for CD117 (ckit) (Miltenyi Biotec). ckit+ BM cells were pre-stimulated for 24 h in CellGro media (Corning) supplemented with murine stem-cell factor (*m*-Scf, 50 ng/ml, Peprotech) and murine thrombopoietin (*m*-Tpo, 50 ng/ml, Peprotech). Retroviral particles were produced using standard protocols and an ecotropic envelope using Fugene. Lentiviral particles were produced by transient transfection with the lentiviral plasmid together with pSPAX and VSVG packaging plasmids using Fugene. Lentivirus and retrovirus particles were concentrated via ultracentrifugation at 4°C. Retroviral transduction was performed on retroNectin (Takara Bio)-coated cell culture dishes pre coated with unconcentrated virus with the addition of concentrated retroviral supernatant in the presence of 4 μg/ml polybrene at 37°C for at least 24 h. Lentivirus transductions were performed with concentrated lentiviral supernatant in the presence of 4 μg/ml polybrene at 37°C for at least 24 h.

Flow cytometry

Patient PBMCs were defrosted, washed in 2%FCS/PBS (Gibco) and passed through a 70um cell strainer to remove clumps. Cells were stained with the following extracellular monoclonal, directly fluorochrome-conjugated antibodies; anti-human: CD19 (BB700, BD, 1:100), CD66b (PE, BD, 2.5:100), HLA-DR (PeCy7, BD, 1:100), CD45 (APC-H7, BD, 2.5:100), CD3 (BV510, BD, 1:100), CD88 (BV786, BD, 1:100), CD89 (BV786, BD, 1:100) in the dark at 4°C for 30 min before fixation and permeabilization of the cells (Transcription Factor Buffer Set, BD) and staining the with intracellular Gli1 antibody (AF647, Novus Biologicals, 1:200) according to manufacturer's protocol.

Peripheral blood collected during animal experiments was first lysed with Pharm Lyse (BD) for 15 min at RT, washed with 2%FCS/PBS (Gibco) and stained using CD3 (PE, BioLegend), CD41 (PeCy7, BioLegend), GR1 (ef450 ThermoFisher), CD11b (APC, BioLegend), CD45.1 (APCCy7, BioLegend), CD45.2 (PerCPCy5.5, BioLegend).

At sacrifice murine BM cells were isolated by crushing the pelvis, hind leg bone and spine in 2%FCS/PBS before being strained through a 70μm cell strainer. BM was lysed at RT for 10 min with red blood cell lysis buffer (BD Pharm Lyse) before being washed in 2%FCS/PBS. Cells were labeled 1:100 in 2%FCS/PBS for 15 min in the dark at 4°C with the following monoclonal directly labeled antibodies; anti-mouse: CD3 (PE, BioLegend), CD41 (PeCy7, BioLegend), GR1 (ef450, ThermoFisher), CD11b (APC, BioLegend), CD45.1 (APCCy7, BioLegend), CD45.2 (PerCPCy5.5, BioLegend), ckit (APC, BioLegend), Sca1 (PerCPCy5.5, Sony BioTech), CD48 (APCCy7, BioLegend), CD150 (PeCy7, BioLegend), CD45.2 (PE, Sony BioTech), CD3 (ef450, ThermoFisher), B220 (ef450, ThermoFisher), CD11b (ef450, ThermoFisher), GR1 (ef450, ThermoFisher), Ter119 (ef450, ThermoFisher).

All samples were analyzed/sorted by flow cytometry using a FACSCantoII, FACSFortessa FACSMelody or FACSAria (BD Biosciences) and data were analyzed using FlowJo Software (Version10, TreeStar Inc), MFI of Gli1 values were corrected for FMO values in all experiments.

Stimulation of HD PBMCs

PBMCs were cultured in RPMI with 10% FCS and 1% Pen/Strep with added SCF (100 ng/ml), IL3 (30 ng/ml), IL-6 (25 ng/ml) and FLT3L (50 ng/ml) as a base medium. Prior to and during stimulation the FCS concentration was reduced to 1%. Cells were stimulated with 50 ng/ml IL-6 or 10 ng/ml TGFb1 for 72 h and the stimulation was refreshed every 24 h. At the end of the experiment cells were collected, washed and processed for transcription factor FACS as described above.

Human megakaryocytic cell line culture

MEG-01 cells were maintained in 90% RPMI 1640 (Gibco, #21875-091), 10% FCS and 1% Pen/Strep at a seeding density of 5.0 x 10^5/mL. SET-2 cells were maintained in 80% RPMI 1640, 20% FCS and 1% Pen/Strep at a seeding density of 8.0 x 10^5/mL. Cells were collected and processed for RNA isolation as described below.

Patient-derived IPSC lines and JAK2 conditioned medium

Patient derived IPSC lines and paired JAK2^{WT} and JAK2^{V617F} clones were generated and characterized as described by Satoh et al.,[77] and Vieri et al..[78] Undifferentiated IPSC lines were maintained as described by Olschok et al.[79] Spin embryoid bodies (spin EBs) were generated following a previously established protocol[80] with some modifications as described by Satoh et al.[77] and Olschok et al.[79] Briefly, iPS cells were harvested with Accutase (PAN-Biotech, Aidenbach, Germany) and a single cell suspension was plated at a density of 4-4.5x10^5 cells/well on round-bottom 96-well suspension plates (Greiner) serum free medium (SFM) containing 10 ng/mL BMP4 (Miltenyi Biotec), 10 ng/mL bFGF (Peprotech), 10 μM Y-27632 (Abcam), 50 μg/mL L-ascorbic acid (L-AA, Stemcell Technologies) and 6 μg/mL holo-transferrin (Sigma). SFM was a 1:1 mixture of IMDM and F12 medium (both Thermo Fisher Scientific) containing 0.5% BSA, 2 mM GlutaMAX, 1% chemically defined lipid concentrate (both Thermo Fisher Scientific) and 400 μM 1-thioglycerol (MTG, Sigma). On d2 fresh medium supplemented with BMP4, bFGF, L-AA, holo-transferrin, and 10 ng/mL VEGF (Peprotech) was added. From d3 onwards, daily half medium changes were performed with medium containing BMP-4, bFGF, VEGF, L-AA, holo-transferrin, and SCF 200 ng/ml. From d7 BMP4 and VEGF were withdrawn, and from d12 bFGF was withdrawn and 20 ng/mL TPO (Miltenyi Biotec) was added to medium. On d14 medium was collected, centrifuged, diluted 1:1 with sterile PBS, filtered through a 0.2um filter to remove cell debris and frozen for use in stimulation experiments.

Murine hematopoietic progenitor cell lines and ThPO conditioned medium

HOXB8 multi potent progenitor cells were generated from WT whole bone and maintained according to the protocols described by Xu et al.,[81] they were subsequently transduced with ThPO lentiviral particles generated as described above and sorted for GFP positivity. Cells were cultured at a density of 0.5x10^6 cells/ml for 72h before medium was collected centrifuged, filtered through a 0.2um filter to remove cell debris and frozen for use in stimulation experiments.

Generation of hMSC cell line, subsequent recombinant cytokine and conditioned medium stimulation

BM stromal cells isolated from healthy patient femur head samples were isolated as previously described[29] and immortalized using hTERT and LargeT over expression vectors.[70–72] Cells were cultured in AlphaMEM (CytiviaHyClone) supplemented by 10% FCS, 1% Pen/Strep, 1%Sodium Pyruvate (Gibco) and 1% HEPES (Gibco) (full medium). On Day 0, 90′000 cells were seeded in one well of a 6-well plate (TPP) (n = 3 per condition) in full medium. After allowing for attachment overnight, the full medium was exchanged for starvation medium containing 1%FCS for 24 h.

For TGFb stimulation and Apitosilib experiment: on day 2 cells were pretreated with 5μM Apitosilib (MedChemExpress) or DMSO (in equal proportions) for 1 h in full medium, prior to stimulation with 10 ng/ml rTGFB (Invivogen). Medium (full medium containing +/− 5μM Apitosilib (dissolved in DMSO), +/−DMSO, +/− rTGFB) was refreshed on day 3 after 24 h and cells were collected for RNA isolation by trypsinization (Gibco) and pelleting, on day 4 after 48 h total treatment time.

For conditioned medium and ISO-1 experiment: on Day 2, starvation medium was replaced with conditioned medium generated as described above supplemented with an additional 10% FCS +/− 40μM ISO-1. Cells were cultured in these conditions before being collected for RNA isolation by trypsinization (Gibco) and pelleting, on day 4 after 48 h total treatment time.

Isolation of primary murine MSCs and subsequent stimulation with ThPO conditioned medium

CD74$^{-/-}$ or WT primary MSCs were isolated and cultured according to the protocol previously described by Zhu et al.[82] and were maintained in AlphaMEM (CytiviaHyClone) supplemented by 20% FCS, 1% Pen/Strep, 1 ng/ml murine basic FGF (Peprotech) and 5 ng/ml murine EGF (Peprotech) (full medium). On Day 0, 50′000 passage 3 cells were seeded in one well of a 6-well plate (n = 3 per condition) in full medium. After allowing for attachment overnight, the full medium was exchanged for starvation medium containing 1%FCS for 24 h. On day 2, starvation medium was replaced with ThPO conditioned medium generated as described above supplemented with an additional 10% FCS. Cells were cultured in these conditions before being collected for RNA isolation by trypsinization (Gibco) and pelleting, on day 4 after 48 h total treatment time.

Culture and treatment of HEL cell line

JAK2^{V617F} positive HEL cells were cultured in RPMI 1640 (GIBCO) supplemented by 10% FCS and 1% Pen/Strep (full medium) and maintained at a density of 1x10^6 cells/ml. Prior to treatment on Day 0, cells were plated at a density of 1x10^6 cells/ml (n = 3 per condition) and starved overnight in medium with only 2% FCS (starvation medium). On Day 1 cells were treated with either 500nM Ruxolitinib (Selleckchem), 250nM BEZ235 (Selleckchem) or DMSO. After 4 h, the BEZ235 and equivilant DMSO conditions were harvested and cells were processed for RNA isolation. After 24 h the Ruxolitinib and equivalent DMSO conditions were harvested, and cells processed for RNA isolation.

Culture and stimulation of MSOD cell line

MSOD[67] cells were maintained in AlphaMEM (CytiviaHyClone) supplemented by 10% FCS, 1% Pen/Strep (Gibco), 1% L-Glutamine (Gibco) 1% Sodium Pyruvate (Gibco), 1% HEPES (Gibco) and 5 ng/ml FGF2 (Peprotech) (full medium). On Day 0, 6.6x10^5 cells were seeded in a 6 well plate (TPP). On Day 1, full medium was exchanged with the addition of 100 ng/ml recombinant human MIF (Peprotech). On Day 2, cells were harvested for RNA isolation after 24h stimulation. MSODs were kindly provided by Ivan Martin.

Histological staining

After sacrifice murine organs were fixed in 4% paraformaldehyde for 24 h before being transferred to 70% ethanol. Femurs were decalcified in 10% EDTA/Tris-HCl (pH 6.6) solution for 7 to 10 days, dehydrated and paraffin embedded. H&E, Reticulin staining (Sigma-Aldrich) and Sirius red/Fast Green (Chondrex) were performed on 4μm sections according to routine protocols.

scRNA sequencing sample preparation

BM was isolated at sacrifice and frozen at −80°C in 90% FCS +10% DMSO. was defrosted, washed in 2%FCS/PBS before being strained through a 70μm cell strainer. Whole BM cells from each replicate (n = 3) within a group were incubated with 2.5-5μl of hashtag antibody (anti-mouse-TotalSeq, BioLegend) and lineage depletion antibodies (Miltenyi) for 10 min at 4°C. Subsequently, standard magnetic depletion protocol was followed. Eluted Lineage negative cells from each replicate were mixed per group and stained with Celltrace Calcein Red/Orange (ThermoFisher) (viability) for 15 min at RT and anti-mouse; CD3 (ef450, ThermoFisher), B220 (ef450, ThermoFisher), CD11b (ef450, ThermoFisher), GR1 (ef450, ThermoFisher), Ter119 (ef450, ThermoFisher) for 15 min at 4°C to check purity of lineage depletion. Two populations were sorted (BD FACSAriaII); GFP(Jak2)$^{-}$Lin^{-}, to enrich for stromal cells, and GFP^{+}. The populations were mixed 75%/25% respectively and used for the 10x platform.

scRNA library preparation and sequencing

RNA Libraries were prepared using the Chromium Single Cell 3′ Reagents kits (10x Genomics): Chromium Next GEM Single Cell 3' Kit v3.1 (PN-1000268), Chromium Next GEM Chip G Single Cell Kit (PN-1000127), Dual Index Kit TT Set A (PN-1000215). Additional libraries were generated for the hashtags using publicly available protocol.[83] Quality of the libraries was determined using D1000 ScreenTape on a 2200 TapeStation system (Agilent Technologies). Libraries were sequenced on an Illumina Novaseq6000 targeting a read depth as suggested by 10x Genomics 3′ single-cell RNA kits v3.1.

scRNA-seq data—Alignment

Using cell ranger Version 4.0.0, reads were aligned to mouse genome mm10, with an added GFP sequence (5′ATGGTGAGCAAGGGCGAGGAGCTGTTCACCGGGGTGGTGCCCATCCTGGTCGAGCTGGACGGCGACGTAAACGGCCACAAG TTCAGCGTGTCTGGCGAGGGCGAGGGCGATGCCACCTACGGCAAGCTGACCCTGAAGTTCATCTGCACCACCGGCAAGCTGCC CGTGCCCTGGCCCACCCTCGTGACCACCCTGACCTACGGCGTGCAGTGCTTCAGCCGCTACCCCGACCACATGAAGCAGCACG ACTTCTTCAAGTCCGCCATGCCCGAAGGCTACGTCCAGGAGCGCACCATCTTCTTCAAGGACGACGGCAACTACAAGACCCGCG CCGAGGTGAAGTTCGAGGGCGACACCCTGGTGAACCGCATCGAGCTGAAGGGCATCGACTTCAAGGAGGACGGCAACATCCTG GGGCACAAGCTGGAGTACAACTACAACAGCCACAACGTCTATATCATGGCCGACAAGCAGAAGAACGGCATCAAGGCGAACTTC AAGATCCGCCACAACATCGAGGACGGCAGCGTGCAGCTCGCCGACCACTACCAGCAGAACACCCCCATCGGCGACGGCCCCG TGCTGCTGCCCGACAACCACTACCTGAGCACCCAGTCCGCCCTGAGCAAAGACCCCAACGAGAAGCGCGATCACATGGTCCTG CTGGAGTTCGTGACCGCCGCCGGGATCACTCTCGGCATGGACGAGCTGTACAAGTAA) and cells detected using default parameters.

scRNA-seq data—Initial processing

All primary scRNA-seq analysis was performed using the Seurat[73] toolbox (v4.0.1) for R (v4.0.5)

Data from all cells underwent uniform preprocessing for quality control, using standard thresholds of <10% mitochondrial reads and <30000 total counts. Normalization was carried out, involving variance-stabilizing log2 transformation and regression of technical factors (number of counts and percentage of mitochondrial reads).

Cells were demultiplexed according to hashtag antibodies which were unique to each biological replicate. This was done using HTODemux (included in Seurat) according to kmeans clustering with a threshold of 0.99. Preliminary visualization of the data following hashtag demultiplexing revealed high lineage bias in one control (WT + $Jak2^{WT}$) replicate. This replicate was not included in any subsequent downstream processing and analysis. Due to the overall low efficiency of hashtagging we did not separate the biological replicates for downstream analysis.

Ambient RNA contamination was estimated using the SoupX package[74] (v1.5.0). Filtering was applied to eliminate the top 0.1% of genes identified as contamination, with the notable exception of S100a8 and S100a9 which were retained due to known biological relevance in the context of fibrosis.[26] Mitochondrial genes and X-linked long non-coding RNA genes were also removed due to visible biases. We chose not to regress out cell cycle as no projections suggested a cluster specific cell cycle bias and we wanted to preserve any knockout mediated effects. Datasets were then integrated using rpca integration. See Table S2 for quality control thresholds, metrics and cell numbers for this dataset.

scRNA-seq data—Cluster annotation

Unsupervised clustering of cells was performed using UMAP dimensionality reduction, and clusters were annotated according to consensus across multiple differential expression analyses. Marker genes for each cluster were identified using the FindMarkers function included in Seurat. These markers were interrogated via gene enrichment using WebGestaltR[30] (v0.4.4), as well as comparison to known markers using cellmarkersDB[28] (v1.0.0) and previously published markers.[29] The same FindMarkers function was used to identify the differential genes between individual conditions, statistics of which were used to generate plots in Figures 4 and S4.

scRNA-seq data—Transcription factor analysis

Transcription factor activity prediction was performed via enrichment analysis with the DoRothEA gene regulatory network[53] (v1.7.2). Based on the expression matrix of the scRNA-seq data, transcription factor activity scores were retrieved using the statistical method provided within the DoRothEA R package. For each cell, the predicted transcription factors were returned with a corresponding activity score, in the form of z-scores for comparability. By grouping the cells based on the cell type or sample condition and averaging over the activity scores for each transcription factor, the analysis of differences between the groups was enabled.

scRNA-seq data—Pathway activity analysis

For pathway analysis, we used FindMarkers function with logfc.threshold >0.25 to find condition and cluster specific markers. Pathway enrichment analysis was performed using the enricher() function from clusterProfiler[76] (v3.18.1) and Hallmark gene sets.[42]

scRNA-seq data—Ligand-receptor analysis

Ligand receptor interactions representing cell-cell communication were identified for each individual normalized and preprocessed dataset using CellPhoneDB[75](v2.1.7) considering only the interactions with p value $\leq$ 0.05. CrossTalkeR[53] (v1.3.2) was used to was used to build and analyze ligand-receptor derived networks and shed light on interactions which differ between conditions, as well as generating network plots.

RNA isolation and RT-qPCR analysis

Cell pellets were immediately processed using the NucleoSpin RNA Plus XS kit (Macherey-Nagel) or the RNAeasy kit (Quiagen) as per manufacturer's instructions. 1μg eluted RNA was reverse transcribed into cDNA using the High-Capacity cDNA Reverse Transcription Kit (Thermo-Fisher). Quantitative polymerase chain reactions were performed using Applied Biosystems Fast SYBR Green Master Mix (Applied Biosystems) on a CFX Opus 96 system (BioRad). HPRT1 was used as a house-keeping gene and the $2^{-\Delta\Delta CT}$ method to calculate differences in RNA levels.

Primer sequences

	Human rt-qPCR	
	FW	RV
HPRT1	CCTGGCGTCGTGATTAGTGA	CGAGCAAGACGTTCAGTCCT
COL1a1	ATCAACCGGAGGAATTTCCGT	CACCAGGACGACCAGGTTTTC
GLI1	CGGGGTCTCAAACTGCCCAGCTT	GGCTGGGTCACTGGCCCTC

(*Continued on next page*)

Continued		
	Human rt-qPCR	
	FW	RV
GAPDH	GAAGGTGAAGGTCGGAGTCA	TGGACTCCACGACGTACTCA
TNFa	TGCACTTTGGAGTGATCGGC	CTCAGCTTGAGGGTTTGCTAC
TGFb1	GGTGGAAACCCACAACGAAAT	GAGCAACACGGGTTCAGGTA
MIF	GCCGCGTTCATGTCGTAATA	GCGCCTGCGCATCAG
	Mouse rt-qPCR	
	FW	RV
aSMA	CTGACAGAGGCACCACTGAA	CATCTCCAGAGTCCAGCACA
Gli1	ATCACCTGTTGGGGATGCTGGAT	CGTGAATAGGACTTCCGACAG
Gapdh	AGGTCGGTGTGAACGGATTTG	TGTAGACCATGTAGTTGAGGTCA

ELISA

Before use, samples were thawed gently on ice and centrifuged for 5 min at 2500xg. Serum samples were diluted 1 in 10 and MIF concentration was quantified using the LegendMax Human Active MIF ELISA kit (BioLegend) according to manufacturer's instructions. For SHH concentration, Plasma samples were used undiluted and quantified using the Human Sonic Hedgehog/Shh N Terminus DuoSet ELISA (R&D).

QUANTIFICATION AND STATISTICAL ANALYSIS

Image processing and quantification

All plots were generated with GraphPad Prism Version 9.0.0 or R Version 4.2.0. To ensure readability line thickness, labels and font size were adjusted manually using Adobe Illustrator CC 2023. Size, count and area quantification from images was performed via ImageJ from a minimum of 3 representative fields per section. BM composition was analyzed from whole sample scans of H&E stained slides using *MarrowQuant*.[47] Unless otherwise specified, images were representatively chosen and jointly rescaled before manual alignment.

Statistical analysis

Statistical analysis – excluding that for scRNAseq data – was performed using GraphPad Prism version 9.0.0. Correlation was assessed via simple linear regression testing. Comparison between two groups was performed using an unpaired t test with Welch's correction. For multiple group comparison at a single time point, a one-way ANOVA with post-hoc Tukey correction was applied. For multiple group comparison over multiple time points, two-way ANOVA with Geisser-Greenhouse correction followed by Tukey's post-hoc test was applied. p values lower or equal to 0.05 were considered statistically significant and data are shown as mean ± SEM.